Insights into mountain precipitation and snowpack from a basin-scale wireless-sensor network

Z. Zhang[1], S. Glaser[1], R. Bales[1,2], M. Conklin[2], R. Rice[2] and D. Marks[3]

[1]Department of Civil and Environmental Engineering, University of California, Berkeley.
[2]Sierra Nevada Research Institute and School of Engineering, University of California, Merced.
[3]Agricultural Research Service, USDA, Boise.

Key Points:
- **Distributed sensor data captures spatial heterogeneity in rain versus snow precipitation that is not apparent in more limited operational data**
- **Distributed dew-point temperature measurements provide accurate estimates of snow-rain transition elevation during storms**
- **Distributed, representative measurements can improve operational estimates of snowpack water storage and melt across the basin**

Abstract

A spatially distributed wireless-sensor network, installed across the 2154 km^2 portion of the 5311 km^2 American River basin above 1500 m elevation, provided spatial measurements of temperature, relative humidity and snow depth in the Sierra Nevada, California. The network consisted of 10 sensor clusters, each with 10 measurement nodes, distributed to capture the variability in topography and vegetation cover. The sensor network captured significant spatial heterogeneity in rain versus snow precipitation for water year 2014, variability that was not apparent in the more-limited operational data. Using daily dew-point temperature to track temporal elevational changes in the rain-snow transition, the amount of snow accumulation at each node was used to estimate the fraction of rain versus snow. This resulted in an underestimate of total precipitation below the 0 ^{o}C dew-point elevation, which averaged 1730 m across 10 precipitation events, indicating that measuring snow does not capture total precipitation . We suggest blending lower-elevation rain-gauge data with higher-elevation sensor-node data for each event to estimate total precipitation. Blended estimates were on average 15-30% higher than using either set of measurements alone. Using data from the current operational snow-pillow sites gives even lower estimates of basin-wide precipitation. Given the increasing importance of liquid precipitation in a warming climate, a strategy that blends distributed measurements of both liquid and solid precipitation will provide more accurate basin-wide precipitation estimates, plus spatial and temporal patters of snow accumulation and melt in a basin.

Index Terms and Keywords: Wireless-sensor network, rain-snow transition, mountain precipitation, mountain snow

1. Introduction

At the basin scale, measurements of mountain water cycles currently are limited in both spatial coverage and temporal resolution, with data largely provided by a few operational precipitation, snowpack, climate and stream-gauging stations [Bales et al., 2006; Dozier, 2011]. In the Sierra Nevada, measurement sites tend to be limited to middle and lower elevations and flat terrain in forest clearings [Molotch and Bales, 2005]. Research networks include a few selected headwater basins where a more complete set of meteorological and hydrologic attributes are accurately measured [Kerkez et al., 2012]. While these catchments offer some detailed information on mountain hydrology, they provide a limited understanding of the hydrology of larger mountain river basins that can be characterized by steep gradients in temperature, precipitation, and rain versus snow fraction. In mountainous environments, the interaction between soil, vegetation, and existing snowpack and precipitation depends strongly on the precipitation phase [Kormos et al., 2014]. One of the common ways to determine the phase of precipitation is through a calibrated model of air temperature. However, the precipitation phase and air temperature relationship is higher variable across different seasons, sites, and storm tracks, while

dew-point temperature shows a strong relationship to precipitation phase [Marks et al., 2013].

Operational forecasts of runoff are sensitive to estimation of rain versus snow, as illustrated by a tripling of storm runoff for a 600-m change in the estimated melting-level elevation in one simulated 24-hour precipitation event in the American River basin [White et al., 2002]. Rain-snow transition elevation, or freezing levels, are of particular interest for warm events, and it has been observed that forecast biases associated with freezing levels above 2300 m in the basin have been underestimated by as much as 900 m [White et al., 2010]. It has been noted that the rain–snow transition region is of great scientific as well as practical interest, affecting both current forecasting and potential improvements in predictive tools [Ralph et al., 2005].

Mesoscale differences between the atmospheric 0° C elevation and the mountainside snow line in the Sierra Nevada make both characterizing and predicting the snow line particularly challenging. Data from three years of storms show that the mesoscale lowering of the snow line is a feature common to nearly all major storms, with an average snow-line drop of 170 m [Minder and Kingsmill, 2012]. While radar can be an effective tool for detecting rain versus snow, and other attributes of a precipitation event, its use is limited in the complex topography of the upper American River basin [Matrosov et al., 2007].

Combining dew-point temperature with air temperature has previously been shown to provide a reliable estimate of the timing and phase of precipitation [Marks et al., 2013]. Precipitation occurs when temperature approximately equals dew-point temperature, indicating saturation of an air parcel. The critical temperature range of separating solid versus liquid is usually wider and more variable for a method based on air temperature compared to one based on dew-point temperature. Therefore, using a dew-point temperature-based method to determine the phase of precipitation is generally less geographically dependent [Ye et al., 2013]. It has also been observed that using ground-based dew-point temperatures to determine the phase of precipitation is potentially more accurate than radar-based methods due to reduction of error associate to interpreting the radar measurement [Lundquist et al., 2008].

Recently developed and deployed wireless sensor network (WSN) clusters in the American River basin provide a rich dataset with significantly denser spatial sampling than operational stations. This richer dataset allows us to understand and characterize the critical gradients in temperature, humidity, and precipitation that help define the dynamics of mountain water balance. It can enable use of new classes of spatially explicit hydrologic-modeling tools to produce quantitative assessments, influence hydrologic forecasting, probe system response to climate and land-cover perturbations, increase process understanding of basin-scale water cycles, and provide defensible scenarios for infrastructure planning over a scale currently not possible. These WSN clusters complement deployments by others to monitor extreme weather events for flood forecasting [White et al., 2013].

The specific aims of the research reported in this paper are to assess how spatially distributed sensor-network data can improve estimates of: i) the basin's average rain-snow transition elevation during precipitation events, ii) the amount of rain versus snow during mixed-precipitation events across the basin, and iii) the amount and timing of snowmelt across the basin. Together, these affect the soil-moisture and runoff patterns across a basin.

2. Methods

Data from 80 wireless-sensor nodes distributed in 10 strategically chosen networks in the American River basin were used together with operational data to estimate precipitation as rain versus snow, snow ablation, and melt, across the upper part of the basin for the 2014 water year. Although a drought year, there were 11 events with measurable precipitation, 10 of which were used in the current analysis. The sensor-network nodes provided temperature, relative humidity and snow-depth data across the range of topographic and vegetation characteristics in the portion of the basin where snow is currently an important part of the water balance.

2.1 Study area

The study area was the American River Hydrologic Observatory, a spatially distributed water-balance WSN in the upper, snow-dominated part of the American River basin on the western slope of the Sierra Nevada in California (36.069 N, -120.583

W). The basin is incised with steep river canyons and comprises three sub-basins: the North, Middle, and South forks, which combine to form a drainage basin of 5311 km^2. Basin elevations range from 200 m at Folsom Reservoir to 3100 m at the Sierra crest, with precipitation transitioning from rain to snow at about 1400-1600 m [Raleigh and Lundquist, 2012; Klos et al., 2014]. Sixty percent or about 2154 km^2 of the basin is above 1500 m, the location of the WSNs. The basin supports diverse vegetation types ranging from grasslands, oak woodland, chaparral, and oak savannas at the lower elevations, mixed conifers and montane hardwoods at the mid to upper elevations, and above the montane forest is the sub-alpine, alpine meadows, and shrub land [Van Wagtendonk and Fites-Kaufman, 1997]. The canopy structure exhibits high heterogeneity in both percent coverage and vegetation type, as indicated by National Land Cover Database [Jin et al., 2013]. The forest landscape is subjected to land-cover perturbations such as forest thinning and fire.

Locations for both the ten sensor network clusters, with each cluster distributed over approximately 1.5-km^2 area and up to ten sensor nodes within each cluster, were placed in physiographically representative regions to capture the variability of the upper basin (Figure 1). Each sensor node is equipped with an ultrasonic snow-depth sensor (Judd Communication Depth Sensor) and a temperature/relative humidity sensor (Sensirion SHT-15). See Table 1 for locations and other information on the ten clusters of nodes used.

2.2. Data

Data were from two sources, WSNs and operational stations. Time-series data were taken from 80 sensor nodes of the sensor-network clusters for the first eight months (Oct-May) of the 2014 water year (WY). Nodes in each of the 10 clusters were placed within a 1-km^2 area to capture the variability in vegetation cover, aspect and slope. Each node was sampled at 15-minute intervals for snow depth, temperature and relative humidity. Hourly and daily products for each attribute were developed by averaging the 15-minute data. Precipitation, temperature, snow depth and snow water equivalent (SWE) from across the basin were acquired from operational stations. All data were subjected to quality control to remove noise, following the protocols described in *Daly et al.* [2008]. Hourly and daily products were developed for periods where no less than 75% of data were valid within the averaging window. Precipitation data were not adjusted for gauge undercatch, which should be relatively small in these densely forested areas.

In order to estimate SWE from sensor-network measurements of snow depth, we used a basin-averaged snow density derived from ten snow-telemetry sites where snow depth and SWE were both measured. The sites range in elevation from 1901 to 2546 m, similar to the 1518-2673 m elevation range of our WSNs (see Table S1). Because 2014 was a drought year, there was insufficient snow to measure density over the season below 1900 m elevation. A density time series was developed using the ratio of daily SWE and snow depth (See Figure S1). Density values from all sites were averaged, and this mean-density time series used for SWE calculations at all sensor-network nodes, with mean values ranged from about 130 kg m^{-3} in January to 420 kg m^{-3} in May At the beginning of the season when the snow pillow may have been only partially covered, density was assumed to be 330 kg m^{-3}, the seasonal average. Near the end of the season, the last valid snow-density value from each site was extrapolated to calculate basin-average snow density. . There was no apparent elevation pattern to the density record, which is consistent with our past analyses [Kirchner et al., 2014].

2.3. Precipitation phase and rain-snow transition elevation

The total amount of precipitation for each of the 10 main precipitation events was estimated for each sensor-network node using the changes in accumulated snow and dew-point temperature. One event, in early May, was not included owing to the very small amount of precipitation. Solid precipitation at each node was computed as the sum of the daily increase in snow depth over the duration of the storm event, times the daily density value. Dew-point temperatures were calculated at each node based on an empirical formula [Lawrence, 2005], using air temperature and relative humidity. The duration of each precipitation event was defined as the period when hourly air and dew-point temperatures were within 1^o C. For each day with solid precipitation, the mean daily dew-point temperatures were used to

determine the precipitation phase. The proportion of liquid and solid precipitation was computed from the daily dew-point temperature. For temperatures between $\pm 1^{o}$ C, the proportion of snow and rain was assumed to vary linearly from 0 to 100%. Above $+1^{o}$ C and below -1^{o} C precipitation was assumed to be 100% rain (liquid) or snow (solid). We refer to this as the dual-temperature method. We thus defined the rain/snow transition zone as the band of elevations between $\pm 1^{o}$ C dew-point temperature. Precipitation results from the WSNs were evaluated using measurements of SWE from snow pillows and precipitation from rain gauges at two sites (ALP and ECP). While a non-linear relationship between monthly air temperature and fraction rain or snow in precipitation has been developed and used with rain-gauge data, we did not have sufficient data to develop that sort of relationship here [Ohmura et al., 1999; Bales et al., 2009].

2.4. Basin mean SWE and melt

The amount of accumulated snow and melt-out dates provide an additional check on the partitioning of rain versus snow precipitation. Spatially averaged sensor-network SWE estimates were compared to operational snow data to assess differences in melt patterns and melt-out dates across elevation. The portion of the basin above 1500 m was divided to three elevation zones of equal area, with cutoff elevations at 1752 m and 2041 m. The basin's area/elevation relationship was derived from a 30-m DEM. SWE estimates from sensor nodes in each zone were averaged to zone and basin means. The snow-disappearance day for each node was determined as the day snow depth fell below 1 cm.

3 Results

3.1 Temperature, humidity and precipitation

Data from the 80 measurement nodes illustrate both within-cluster heterogeneity and average patterns across different elevations within the basin. For example, within a cluster the daily cycle of air temperature for the 10 nodes at ALP (Figure 2a), over a typical 14-day period, showed a $5\text{-}10^{o}$ C difference between hourly maximum and minimum values on a given day, with temperatures below 0^{o} C during snow accumulation (Figure 2c). The smallest snow accumulation during the event on water-year day (WYD) 207 was 22 cm for a node in a heavily forested location, with two other nodes (in the forest clearing) receiving 31 cm of snow. Relative humidity peaked at 100% from WYD 206 to 208 (Figure 2b), and showed little variability across the site. Most of the snow disappeared within three days after the event due to warm temperatures.

Across the basin, eight of the 10 clusters of nodes were co-located with a met station (Table 1), and Figure 3 provides a comparison between the sensor-network spatial mean versus single met-station temperature. At four of these, the met-station average temperature was within 1^{o} C of the 10-node average. Over an 8 month-period, at four of the clusters (BTP, VVL, CAP, ECP) the average daily sensor-network temperature was 1.5, 1.1, 1.1 and 1.8^{o} C, respectively, below that for the nearby operational station (see Figure 3). For these sites, 80%, 2%, 58% and 77%, respectively, of days had a difference greater than 1^{o} C between the network mean and the station.. Four of the ten sites also have an operational station with a shielded rain gauge to measure precipitation, plotted as daily values on Figure 3. Note that precipitation was recorded for most, but not all events at these sites.

3.2. Rain-snow transition zone

The rain-snow transition zone falls within the elevation range of our sensor network for nine out of 10 precipitation events (Table 2), ranging in elevation from 1463 to 2011 m. The exception was a cold event on WYD 67 (Event E3), with an average daily dew-point temperature of -13.5^{o} C, and maximum of -9.1^{o} C. During this event, the rain-snow transition was at 627-m elevation, well below all of our sensors. The rest of the events all had 0^{o} C dew-point temperature elevations between the highest and lowest of our sensors (Figures 4 and S2.1a-S2.9a). Placement of WSNs above 1518 m was sufficient to define the rain-snow transition for most events.

The event E6, one of the largest multi-day snow events in water-year 2014, is used as an illustration of our analysis. The $+1^{o}$ C and 0^{o} C dew-point temperatures, presented by Figure 4a, show that the average lower boundary of the rain-snow transition zone ($T_d = 1^{o}$ C) for the five-day period of event E6 was 1681 m. During this event, the rain/snow transition zone gradually moved up in elevation. The hourly dew-point lapse rates (Figure

4b) during precipitation were relatively stable (mean -5.0° C km^{-1}) compared to pre-and post-event values, with R^2 values (Figure 4c) significantly higher and RMSE (Figure 4d) lower during precipitation. Early in the event, snow depths recorded at all clusters tracked each other, with a divergence of trends observed on WYD 131, when only the half of the clusters at higher elevation recorded increases in snow depth (Figure 4e). For comparison, at operational station FRN (2269 m elevation) the precipitation gauge recorded 5 cm on WYD 130, with no SWE increase recorded on the snow pillow (Figure 4f). Concomitantly, operational station ECP, roughly 200 m higher in elevation, recorded a 15-cm increase in SWE and 13-cm increase in precipitation during the same day (Figure 4f). Both sites received solid precipitation on WYD 132 as the storm intensified.

The basin-wide upslope migration of the rain/snow transition during event E6 was observed in the daily increase of snow-depth measurements. The lower-elevation nodes gradually lost recordable snow starting from WYD 130 (Figure 4g). Migration of the snow line coincided with the upward movement of the zero dew-point temperature (Figure 4a). The mean hourly difference between air temperature and dew-point temperature was 0.4° C during the four-day event (Figure 4h). The air remained relatively saturated across elevations and time span of the entire event.

Similar records for other events are shown in supplemental Figures S2.1 to S2.9. The mean R^2 of the dew-point-temperature lapse rate for all 10 events was 0.78 and the RMSE was 149 m, indicating an overall good fit of the dew-point data during the precipitation events.

The amount of solid and total precipitation by event is shown in Figure 5a for each node and in Table 3 for the basin average above 1500 m. The rain fraction was higher at lower elevations, with considerable variability across the nodes of each local cluster owing to local differences in dew-point temperature. A precipitation lapse rate for each event was calculated as the slope of the linear best-fit line. The values for solid precipitation lapse rate varied from 1-3 cm km^{-1} in events E3, E4 and E10, all relatively small events compared to over 30 cm km^{-1} in the largest event E6 (Table S2). All slopes in Figure 5a were statistically significant ($p < 0.05$), except total precipitation for event E8 ($p=0.27$). For binned data, events E3 and E8 had $p > 0.05$ (0.08, 0.11, respectively), with the other eight events having statistically significant fitted lines. Solid precipitation lapse rates for the binned data were on average about 0.6 cm km^{-1} higher than for all-node data. The analysis shown on Figure 5b uses 11 bins of 100-m in elevation; results were essentially the same for fewer bins (data not shown). Doing the same analysis of total and liquid precipitation using snow-pillow data, together with dew-point temperature from the wireless-sensor nodes (Figure 5b), gives lapse rates that are about 2.3 cm km^{-1} lower than those for the binned node data, and on average differ from the slopes for the node data by about 25%. Differences between binned-node and snow-pillow data were all relatively large for the two events with the steepest precipitation lapse rates, events E6 and E7. Using rain-gauge data gave precipitation lapse rates that were near zero, and in some cases negative for the 10 events (Table S2). Only one event (E5) had a statistically significant trend. The relatively small number of well-maintained, representative sites limits use of rain-gauge data, especially at higher elevations.

Normalizing precipitation lapse rates by the mean precipitation amounts in Table S2 gives values of about 2.4 $\pm$ 1.8 km^{-1} (mean $\pm$ standard deviation) for all nodes, versus 2.2 $\pm$ 1.0 km^{-1} for binned data, and 2.0 $\pm$ 1.3 km^{-1} for the snow-pillow data. On average, normalized precipitation lapse rates for each event differed by about $\pm$33% for the sensor-node versus snow-pillow data. Normalized total precipitation lapse-rate values for sensor-node data range from 0.3-0.8 for E1, E3, E8 and E9 to 2.5-3.2 for E4, E6 and E7 to 3.7-5.1 for E2, E5 and E10.

The contribution of liquid precipitation for mixed rain-snow events can be significant. For example, during event E6 2.8 cm of liquid precipitation, averaged across elevations, was recorded, with 9.3 cm solid precipitation by the nodes (Table 3). Using the node data, it is estimated that across the 10 events, about 11% of the estimated total 62 cm of precipitation above elevation 1500 m fell as liquid. However, this likely underestimates the rain contribution to total precipitation at some of the lower sensors owing to the small amount and high variability of solid precipitation. Rain-gauge data, averaged over the basin and summed for all 10 events, give 79 cm

total. Using binned node data gives only 57 cm total precipitation (11% liquid), and snow-pillow data give 52 cm total (15% liquid).

Overall results for the 10 events shown on Figure 5 show similar patterns for WSN versus snow-pillow estimates of solid precipitation for some events; for other events the snow-pillow data fail to show the consistent elevation trend seen in the WSN data. For total precipitation, the WSN and rain gauges show different elevation patterns (Figure 5c); and a blended product would combine lower-elevation rain-gauge data with higher-elevation snow data to provide the most accurate elevational estimate of total precipitation.

3.3. SWE and snowmelt

SWE data show a clear elevation trend, with variability increasing with elevation (Figure 6). Maximum SWE occurred around April 1. During the warm and dry 2014 snow season, snow cover accumulated mainly at elevations above 2100 m. At elevations below that, snow melted soon after a precipitation event. At peak accumulation, average SWE measured by the WSN for the 2154 km^2 above 1500 m was 24.7 cm. Thus the estimated water stored in the snowpack at the American River basin above 1500 m was 532 million m^3 (0.43 million acre feet), or 10 cm averaged across the 5311 km^2 basin. The averages of snow-pillow SWE values showed positive biases when compared to the WSN. However, basin-mean SWE on April 1st from snow courses was 15 cm lower than sensor-network average SWE.

Sites at higher elevations generally had more accumulation and thus a longer melt season compared to lower elevations. For sensor-network sites above 2000 m, snow melt out progressed upslope an average of 13 m day^{-1} (R^2 = 0.68) (Figure 7). This is comparable to the 14 m day^{-1} observed by *Rice et al.* [2011] for a dry year (2004) using satellite snow-cover data. The mean melt-out progressed upslope about 25 m day^{-1} (R^2 = 0.67) if lower-elevation sites were considered. The entire melt season lasted roughly 65 days after April 1 (WYD 183), indicated by the first node at BTP to melt out versus the last node at ECP. The error bars in Figure 7 indicate a 3-22 day variability in the progress of snowmelt among nodes within each cluster. ECP experienced the longest period (61 days) between the first and the last nodes to melt out. The progression of snowmelt within each site was also recorded. Differences in the timing of melt-out between the sensor-network nodes vs. snow pillows were also apparent (Figure 7). Snow-pillow data show an earlier melt out as compared to the cluster means, with 18-, 22- and 30-day differences at VVL, ALP and ECP, respectively.

Related to snowmelt timing, there were significant differences in cumulative temperature (sum of degree days) between sensor-network nodes and met-station sensors, reflecting the placement of WSN sensors capturing the heterogeneity of the landscape, versus placement of the single operational station in a clearing (See Figure S3 for data). For the main snowmelt season, April 4 to June 27, the differences between sensor-network nodes and operational station cumulative values were +24 ^oC-day at VVL, and -68 ^oC-day at ECP. Using an average degree-day factor of 0.4 cm per $^oC^{-1}day^{-1}$ [Shamir and Georgakakos, 2006], the resulting difference in potential snowmelt would amount to about +9.70 cm at VVL and -28 cm SWE at ECP. In contrast, temperature data between the sensor nodes and met-stations from SCN and ALP showed much less difference, +9.7^o C-day and +4.5^o C-day (Figure S3). The differences in potential snowmelt (snowmelt if snow was present) would be +3.9 and +1.8 cm of SWE for SCN and ALP. Further discussion of temperature differences between WSN, operational sensors and model products are in *Zhang et al.* [2017].

4 Discussion

4.1 Dew-point temperature and rain-snow transition

Precipitation data from the nearby rain gauges at ALP and EP5 showed that the dual-temperature method reliably mapped the timing of precipitation (Figure 4g-h). The better characterization of the timing of an event provided by the sensor network helps to estimate event-based indexes such as lapse rate and RMSE more accurately. Reduction of uncertainty in temperature and humidity elevation patterns improves determination of the elevation range associated with the rain-snow transition.

Due to limited relative-humidity measurements at operational stations in the basin, dew-point temperature is not routinely available [Raleigh et al., 2013]. Previous work in the American River basin demonstrated the inaccuracy of estimating daily dew-point temperature patterns

using empirical method-based spatial-projections algorithms, radiosonde data, or PRISM lapse rates [Feld et al., 2013]. They also suggest that dense field measurements or down-scaled atmosphere-model data are two viable solutions to more-accurately estimate daily dew point. Our telemetered sensor-network data are of the density and quality that can support the dual-temperature method.

The bottom of the rain/snow transition elevation, represented as 1° C dew-point temperature, ranged from 627 to 2011 m for the ten events (Table 2). Although the 627-m value was early in the winter, and the 2011 m elevation was later in spring, other values failed to show a consistent increase in elevation from winter to spring. Our range of rain-snow transition elevations was wider than observed at Reynolds Creek, Idaho [Nayak et al., 2010]. *Marks et al*. [2013] did a detailed analysis of the rain-snow transition by putting in place a transect of seven measurement stations providing temperature, humidity and snow depth every 50 m, including precipitation and wind at the bottom (1500 m), top (1800 m) of the catchment, and in a sheltered site just below the top (1750 m) in a 1.8 km^2 sub-drainage within the Reynolds Creek Experimental Watershed. Their work showed that the rain-snow transition is very dynamic moving up and down during mountain storms, and that rain-snow transition level can be reliably determined from site humidity and temperature. However, in the absence of such an extensive measurement network, methods to reliably estimate the rain-snow transition, also referred to as melting level, are still an open question in mountain hydrology [Lundquist et al., 2008]. Widely used snow models such as SNOW-17 are very sensitive to the melting-level parameter input [Maurer and Mass, 2006]. A melting-level error of 500 m can result in a 200% difference in peak flow prediction [White et al., 2002]. Previous studies interpolated ground melting elevation from atmosphere hydrometeor measurements using Doppler-profiling radar [Lundquist et al., 2008; Minder and Kingsmill, 2012]. However, the uncertainty in estimates made from these methods were at best about 300 m in the American River basin. The root mean square error of estimating dew-point temperature was about 150 m using our WSNs (Table 2).

Rain-snow partitioning results are sensitive to the choice of the dew-point temperature thresholds. *Marks et al.*, [2013] proposed a 1° C window, $\pm$0.5 ° C, as the boundary of the transition zone. While they used hourly data for calculation, our study used daily averaged dew-point temperature and SWE in order to mitigate noise in snow depth, possible lags in density data, and the limited availability of hourly precipitation-gauge data. We also use wider bounds, $\pm$1° C, to accommodate uncertainties from measurements and method. The wider bounds allow inclusion of more daily events in the rain/snow transition zone. Specifically, the 100% widening of bounds resulted in an increase in the mean predicted liquid precipitation from 6.2% to 9.9% seasonally and from 14.2% to 21.1% for event E6.

4.2 Partitioning rain and snow

The ability to estimate liquid-precipitation amounts from solid precipitation could substantially extend the current capability of precipitation observations. Those observations are important, as they are the basis of interpolation for some gridded-precipitation products such as PRISM, WorldClim, and Climate Research Unit CL 2.0 [New et al., 2002; Res et al., 2002; Hijmans et al., 2005]. In a study by *Lundquist et al.* [2015], above 2500 m elevation total ground precipitation was assumed to be given by the increase in SWE. Seasonally, the assumption holds for American River site for WY 2014. However, the rain/snow transition zone can reach elevations above 2500 m for warmer event such as E6 (Figure 5). To extent the analysis to lower elevation and higher temporal resolution, accurate temperature or dew-point temperature data are needed to help reduce the uncertainty in predicting the phase of the precipitation.

Besides local spatial variability of dew-point temperature, the temporal variability of dew-point temperature can also produce suitable temperature conditions for snowfall. Event E6 surrounding WYD 131 was an example of such event (Figure 4). On WYD 131, 7 cm of precipitation was recorded at the BTP rain gauge (Figure 3). With a daily averaged dew-point temperature at 3.1°C (Figure 4a), almost all of the precipitation was rain. There was little to no SWE recorded by the five lower WSN clusters (Figure 4e). At higher elevation clusters, almost all of the precipitation was snow. Despite the high mean daily dew-point

temperature, there was still a small but measurable amount of snow deposited at BTP during the event. This was likely due to both the temporal and spatial variability of dew-point temperature, which is not completely captured by a daily, cluster-averaged lapse rate and temperature. An hourly analysis of dew point and precipitation as rain versus snow is feasible using sensor-node data, and there is evidence that use of a finer time step can increase accuracy of phase separation [Harder and Pomeroy, 2013], e.g., melting during the warm part of the day versus freezing at night

On average, the data indicate that up to 89% of the WY 2014 precipitation in these 10 events fell as snow at some of the sensor nodes. The challenges in predicting the amount of liquid precipitation was smaller compared to previous work [Marks et al., 2013]. This is due to the relatively larger elevation differences among sensor nodes, where some higher-elevation nodes receive mostly solid precipitation from all events. Due to lack of solid precipitation in some events at lower elevation, this method could result in under estimating total precipitation and overestimating the precipitation lapse rate.

The general trend of increasing precipitation with elevation followed a less-steep precipitation lapse rate during some events such as events E1, E3, E8 and E9, i.e. higher elevations generally received similar amount of precipitation compared to lower elevations. During those events, elevations account for no more than 27% of the variance in snow deposition.

Four events were associated with atmospheric rivers that made landfall (M. Dettinger 2016, personal communication). Of these, events E2, E6 and E7 had relatively steep precipitation lapse rates. Events E1, E3, E4 and E9 showed no effect of atmospheric river moisture. The outliers are E8, the largest event of the season, which had a weak precipitation lapse rate but was weakly associated with atmospheric-river transport. Smaller events E5 and E10 had steeper lapse rates, but were not associated with land-falling atmospheric rivers.

For 1998-2010, the overall contribution of atmospheric rivers to Sierra Nevada SWE was about 35%, with the rest contributed by less-intense but more frequent precipitation events [Guan et al., 2012]. Eight of the 10 events that we analyzed had ΔSWE in the range of 0.5-4.5 cm day^{-1}, consistent with the observation that 80% of the total SWE for 1998-2010 was contributed by days with ΔSWE in that range [Guan et al., 2010].

4.3 Comparison of basin-wide precipitation estimates

The rain-from-snow reconstruction result was compared to measurements of two co-located sites at EPC and ALP. Both sites simultaneously recorded SWE on a snow pillow and precipitation by a rain gauge. Seasonally, most of the precipitation was estimated as solid at EP5 (co-located with ECP) from the sensor-network data (Figure 8a). Good agreements were observed between the WSN and operational data. At ALP, there were larger uncertainties associated with estimated liquid water content in snow. The snow pillow and precipitation gauge at ALP measured about 25% liquid precipitation versus 12-42% liquid estimated for the sensor-network nodes (Figure 8b). Compared to ECP, ALP is more susceptive to the effects of rain/snow transition due to its lower elevation. Besides the natural heterogeneity, canopy interception and wind redistribution of snowfall to the wireless-sensor nodes at ALP could add sources of uncertainties in predicting liquid water content. These uncertainties may be resolved using subsequent-year data from the WSN, binned and then evaluated using the spatial snow measurements.

Comparing precipitation estimates from operational versus sensor-node data across the basin above 1500 m elevation, it is apparent from comparing Figure 5a and 5b that the 80 sensor nodes capture landscape variability that is not apparent in snow-pillow data. The two data sets give broadly similar precipitation lapse rates (see table S2), the WSN data potentially offer four types of added value. First, the WSN data better capture spatial variability, and thus should give improved estimates of gridded SWE, essential for spatially explicit modeling and forecasting tools. Second, compared to snow-pillow data, the WSN provides redundancy in measurements that can bridge data gaps and uncertainties in snow-pillow measurements. Third, compared to snow-course data, the WSN provides temporally continuous data over the same or larger spatial domain. This is especially important given the shifting rain-snow mix and earlier peak in SWE at snow courses as climate warms. Fourth, these differences together

reduce uncertainty in precipitation, snowpack storage and snowmelt.

It is apparent from Figure 5c that total precipitation estimated using snow depth, and dew-point temperature from the WSN show spatial and temporal differences in precipitation across elevation and other landscape attributes that are not captured by the rain-gauge data. The relationship between precipitation estimates from the two data sets differs for warmer versus colder events. For the colder events E1, E3, E8 and E9, total precipitation estimated by the WSN is higher than that measured in the precipitation gauges. For these four events the rain-snow transition elevation was at or near the 1500-m lower limit of the WSN, and liquid precipitation contributed to the total. For the other six events, the 0^{o} C dew-point elevation was well above 1500 m, and liquid precipitation was more important. A potential limitation of this method is the lack of a verified relationship between fraction rain versus snow and dew-point temperature. A second estimate of total event precipitation comes from combining the two types of measurements, i.e. using precipitation-gauge data at lower elevations and WSN data at higher elevations. Given the few precipitation gauges available in the basin, we used an average value for lower elevations, combining that with WSN data for elevations above that value. The result is higher precipitation estimates for the mixed rain-snow events (Table 3). Over all 10 events, this results in a season total of 90 cm, versus 79 cm for gauges alone and 62 cm for WSN alone. These represent respective total precipitation amounts of 1.9, 1.7 and 1.3 billion cubic meters (1.6, 1.4, 1.1 million acre-ft). A potential value added from this combined estimate is to provide a more accurate elevation dependence of precipitation.

An additional comparison comes from summing precipitation by elevation across all events. Here, we compare two estimates (Figure 9). Note the strong elevation dependence of the WSN estimates versus PRISM data, which is gridded based on operational data. PRISM reflects the mean of precipitation-gauge data in the basin. Here, the point of intersection is about 2400 m, which is still in the snow-dominated part of the basin. Rain-gauge data are shown for reference, and represent part of the data used in the PRISM interpolation. Going forward, improvements in precipitation estimates across the basin should focus more on snow in this region, and rain below. In the mixed rain-snow zone, blending the two should be pursued.

It is acknowledged that the use of a uniform density over the portion of the basin with the WSNs does introduce uncertainty into the estimation of SWE at individual WSN nodes. However, because the snow-pillow sites provide the only reasonable estimate of daily snow density, and the topographic and vegetation structure at those sites do not match those at the WSNs, an effective spatially distributed scheme for distributing snow density from those sites to the WSN's was not feasible. The coefficient of variation for the density values used in this analysis was about 0.20-0.30 early in the season, decreasing to about 0.15 later in the season (Figure S1). These relatively high values are expected for a drought year, when accumulation on snow pillows, where estimates are made, is relatively low. The values are somewhat higher than the average coefficient of variation of 0.08 ± 0.02 found for April 1 density measurements across 14 snow courses in the Merced and Tuolumne basins, over a 60-year period (Figure S4). These same snow courses had an average coefficient of variation of April 1 density of about 0.05 ± 0.02 for the ten measurements within each snow course. Also, over the 60 years analyzed, there was no consistent pattern of density change with elevation, with some years showing a decrease, and very few years having a statistically significant linear trend. While variability in density introduces uncertainty into SWE estimates for individual nodes in the present study, the aggregate uncertainty across the full network is less.

4.4. Basin SWE and snow melt

Similar to prior work, the variability in SWE increases with elevation, but the coefficient of variation showed no distinct trend in elevation at the spatial scale of the WSNs [Perry et al., 2010]. Seasonally, the coefficient of variation for the lower one third of the basin is 1.04, similar to the upper one third at 1.05 (Table 4). The differences in variability at similar elevations can in large part be accounted for by differences in forest canopy coverage [Clark et al., 2011]. At a few higher-elevation sites (e.g. ECP and MTL), the high variability in SWE was caused by high SWE values recorded by a small subset of nodes. The generally lower SWE compared to WSN at co-located snow

pillows reflects sampling bias in snow pillows, versus the more spatially representative sampling of the WSNs [Zhang et al.,2017].

The study characterized the basin's mean SWE by three zones similar to *Welch et al.,* [2013], which showed that strategically placed sensors in three to eight 'clusters' could efficiently characterize SWE in the basin. They recommended measurements taken from clusters with strong elevation differences. Our SWE measurements followed this approach, aimed at producing a representative basin-wide SWE. Continuous measurements at daily temporal resolution can aid in accurately monitoring a basin's hydrologic condition. The combination of dry and warm conditions during WY 2014 places it within the most severe drought periods (WY2012–2014) in the last 1200 years [Griffin and Anchukaitis, 2014]. There were no large storms, and of the few events that occurred, only five deposited snow at all ten sensor-network cluster sites. Snow deposited at lower elevations started to melt as soon as the precipitation event ended. Monthly snow courses at lower elevations missed the timing of those small 'peaks' in SWE for the season (Figure 6).

Reconstruction of SWE backwards from the last day of snow towards the peak accumulation using energy-based methods is of interest to hydrologists for its higher accuracy and robustness to climate change [Guan et al., 2013]. One of the major uncertainties affecting the performance of the method is the knowledge of the snow-disappearance date [Raleigh and Lundquist, 2012]. To determine snow cover, satellite remote-sensing observes snow-covered area, however obstruction of view by cloud cover and canopy are significant challenges for this method. Ground-based sensors can measure snow-covered versus snow-free conditions without that uncertainty. On-the-ground snow and rain measurements can also be used to verify satellite and LiDAR remote-sensing datasets, and account for their limited under-canopy measurements.

5. Conclusions

A spatially distributed wireless-sensor network, installed across the 2154 km^2 portion of the American River basin above 1500 m elevation, reliably provided spatial measurements of temperature, relative humidity and snow depth. This leads to three main conclusions regarding the improvements in accuracy that can be achieved with the network. First, distributed dew-point temperature measurements provided estimates of ground melting levels that were consistent with distributed observations of snow accumulation. These detailed estimates of the elevation of the rain-snow transition are not feasible with current operational sensors; and offer a logistically simpler approach, with lower uncertainty, than prior estimates from deployment of radar in this complex terrain. Second, mixed rain/snow events were common at elevations below 2100 m; and distributed-sensor data showed significant heterogeneity in rain versus snow precipitation that was not apparent in more limited operational data. Using daily dew-point temperature and the amount of snow accumulation at each node to estimate the fraction of rain versus snow resulted in an underestimate of total precipitation below the 0^o C dew-point elevation, which averaged 1730 m across 10 precipitation events, but was as high as 2170 m during one warm event. Rain-gauge measurements failed to capture the elevation and other topographic variability of precipitation. However, blending data from a representative, well-maintained lower-elevation rain gauge with higher-elevation sensor-node data for each event provided precipitation estimates that were on average 15-30% higher than using either set of measurements alone. Given the increasing importance of liquid precipitation in a warming climate, a strategy that blends distributed measurements of both liquid and solid precipitation may provide the most-accurate basin-wide precipitation estimates. Blending data from the current operational rain-gauge and snow-pillow measurements underestimates basin-wide precipitation and snowpack storage. Improving the relationship between dew-point temperature and fraction rain versus snow should also be investigated. Third, distributed, representative measurements also improve upon operational estimates of snowpack water storage and snowmelt amount and snowmelt timing across the basin.

Acknowledgments

The work presented in this paper is supported by the National Science Foundation (NSF) through a Major Research Instrumentation Grant (EAR-1126887), the Southern Sierra Critical Zone Observatory (EAR-0725097), California

Department of Water Resources (Task Order UC10-3), and USDA-ARS CRIS Snow and Hydrologic Processes in the Intermountain West (5362-13610-008-00D). We acknowledge support from the UC Office of the President's Multi-Campus Research Programs and Initiatives (MR-15-328473) through the UC Water Security and Sustainability Research Initiative. Data used to support the analysis can be obtained upon request from the authors or at http://criticalzone.org/sierra/data/.

References

Bales, R. C., N. P. Molotch, T. H. Painter, M. D. Dettinger, R. Rice, and J. Dozier (2006), Mountain hydrology of the western United States, *Water Resour. Res.*, *42*(8), 1–13, doi:10.1029/2005WR004387.

Bales, R. C., Q. Guo, D. Shen, J. R. Mcconnell, G. Du, J. F. Burkhart, V. B. Spikes, E. Hanna, and J. Cappelen (2009), Annual accumulation for Greenland updated using ice core data – 2006 and analysis of daily coastal developed during 2000 – meteorological data, , *114*, doi:10.1029/2008JD011208

Clark, M. P., J. Hendrikx, A. G. Slater, D. Kavetski, B. Anderson, N. J. Cullen, T. Kerr, E. Örn Hreinsson, and R. A. Woods (2011), Representing spatial variability of snow water equivalent in hydrologic and land-surface models: A review, *Water Resour. Res.*, *47*(7), 1–23, doi:10.1029/2011WR010745.

Daly, C., C., W. P. Gibson, G. H. Taylor, G. L. Johnson, and P. Pasteris (2002), A knowledge-based approach to the statistical mapping of climate, *22*, 99–113.

Daly, C., M., Halbleib, J. I. Smith, W. P. Gibson, M. K. Doggett, G. H. Taylor, and P. P. Pasteris (2008), Physiographically sensitive mapping of climatological temperature and precipitation across the conterminous United States, doi:10.1002/joc.

Dozier, J. (2011), Mountain hydrology, snow color, and the fourth paradigm, *Eos (Washington. DC).*, *92*(43), 373–374, doi:10.1029/2011EO430001.

Feld, S. I., N. C. Cristea, and J. D. Lundquist (2013), Representing atmospheric moisture content along mountain slopes: Examination using distributed sensors in the Sierra Nevada, California, *Water Resour. Res.*, *49*(7), 4424–4441, doi:10.1002/wrcr.20318.

Griffin, D., and K. J. Anchukaitis (2014), How unusual is the 2012 – 2014 California drought ?, *Geophys. Res. Lett.*, *41*, 9017–9023, doi:10.1002/2014GL062433.1.

Guan, B., N. P. Molotch, D. E. Waliser, E. J. Fetzer, and P. J. Neiman (2010), Extreme snowfall events linked to atmospheric rivers and surface air temperature via satellite measurements, *Geophys. Res. Lett.*, *37*(20), doi:10.1029/2010GL044696.

Guan, B., D. E. Waliser, N. P. Molotch, E. J. Fetzer, and P. J. Neiman (2012), Does the Madden–Julian Oscillation influence wintertime atmospheric rivers and snowpack in the Sierra Nevada?, *Mon. Weather Rev.*, *140*(2), 325–342, doi:10.1175/MWR-D-11-00087.1.

Guan, B., N. P. Molotch, D. E. Waliser, S. M. Jepsen, T. H. Painter, and J. Dozier (2013), Snow water equivalent in the Sierra Nevada: Blending snow sensor observations with snowmelt model simulations, *Water Resour. Res.*, *49*(August), 5029–5046, doi:10.1002/wrcr.20387.

Hijmans, R. J., S. E. Cameron, J. L. Parra, P. G. Jones, and A. Jarvis (2005), Very high resolution interpolated climate surfaces for global land areas, *Int. J. Climatol.*, *25*(15), 1965–1978, doi:10.1002/joc.1276.

Jin, S., L. Yang, P. Danielson, C. Homer, J. Fry, and G. Xian (2013), A comprehensive change detection method for updating the National Land Cover Database to circa 2011, *Remote Sens. Environ.*, *132*, 159–175, doi:10.1016/j.rse.2013.01.012.

Kerkez, B., S. D. Glaser, R. C. Bales, and M. W. Meadows (2012), Design and performance of a wireless sensor network for catchment-scale snow and soil moisture measurements, *Water Resour. Res.*, *48*(July 2011), 1–18, doi:10.1029/2011WR011214.

Klos, P. Z., T. E. Link, and J. T. Abatzoglou (2014), Extent of the rain-snow transition zone in the western U.S. under historic and projected climate, *Geophys. Res. Lett.*, 4560–4568, doi:10.1002/2014GL060500.

Kormos, P. R., D. Marks, J. P. McNamara, H. P. Marshall, A. Winstral, and A. N. Flores (2014), Snow distribution, melt and surface water inputs to the soil in the mountain rain-snow transition zone, *J. Hydrol.*, *519*(PA), 190–204,

doi:10.1016/j.jhydrol.2014.06.051.

Lawrence, M. G. (2005), The relationship between relative humidity and the dewpoint temperature in moist air: A simple conversion and applications, *Bull. Am. Meteorol. Soc.*, *86*(2), 225–233, doi:10.1175/BAMS-86-2-225.

Lundquist, J. D., P. J. Neiman, B. Martner, A. B. White, D. J. Gottas, and F. M. Ralph (2008), Rain versus snow in the Sierra Nevada, California: Comparing doppler profiling radar and surface observations of melting level, *J. Hydrometeorol.*, *9*(2), 194–211, doi:10.1175/2007JHM853.1.

Lundquist, J. D., M. Hughes, B. Henn, E. D. Gutmann, B. Livneh, J. Dozier, and P. Neiman (2015), High-elevation precipitation patterns: Using snow measurements to assess daily gridded datasets across the Sierra Nevada, California, *J. Hydrometeorol.*, *16*(4), 1773–1792, doi:10.1175/JHM-D-15-0019.1.

Marks, D., A. Winstral, M. Reba, J. Pomeroy, and M. Kumar (2013), An evaluation of methods for determining during-storm precipitation phase and the rain/snow transition elevation at the surface in a mountain basin, *Adv. Water Resour.*, *55*, 98–110, doi:10.1016/j.advwatres.2012.11.012.

Matrosov, S. Y., K. A. Clark, and D. E. Kingsmill (2007), A polarimetric radar approach to identify rain, melting-layer, and snow regions for applying corrections to vertical profiles of reflectivity, *J. Appl. Meteorol. Climatol.*, *46*(2), 154–166, doi:10.1175/JAM2508.1.

Maurer, E. P., and C. Mass (2006), Using radar data to partition precipitation into rain and snow in a hydrologic model, *J. Hydrol. Eng.*, *11*(3), 214–221, doi:10.1061/(ASCE)1084-0699(2006)11:3(214).

Minder, J. R., and D. E. Kingsmill (2012), Mesoscale variations of the atmospheric snow line over the northern Sierra Nevada: Multiyear statistics, case study, and mechanisms, *J. Atmos. Sci.*, *70*(3), 916–938, doi:10.1175/JAS-D-12-0194.1.

Molotch, N. P., and R. C. Bales (2005), Scaling snow observations from the point to the grid element: Implications for observation network design, *Water Resour. Res.*, *41*, 1–16, doi:10.1029/2005WR004229.

Nayak, A., D. Marks, D. G. Chandler, and M. Seyfried (2010), Long-term snow, climate, and streamflow trends at the reynolds creek experimental watershed, Owyhee Mountains, Idaho, United States, *Water Resour. Res.*, *46*(6), doi:10.1029/2008WR007525.

New, M., D. Lister, M. Hulme, and I. Makin (2002), A high-resolution data set of surface climate over global land areas, *Clim. Res.*, *21*(1), 1–25, doi:10.3354/cr021001.

Ohmura, A., P. Calanca, M. Wild, and M. Anklin (1999), Precipitation, accumulation and mass balance of the Greenland ice sheet. With 5 figures, *Zeitschrift fur Gletscherkd. und Glazialgeol.*, *35*(1), 1–20.

Perry, L. B., C. E. Konrad II, D. G. Hotz, and L. G. Lee (2010), Synoptic classification of snowfall events in the Great Smoky Mountains, USA, *Phys. Geogr.*, *31*(2), 156–171, doi:10.2747/0272-3646.31.2.156.

Raleigh, M. S., and J. D. Lundquist (2012), Comparing and combining SWE estimates from the SNOW-17 model using PRISM and SWE reconstruction, *Water Resour. Res.*, *48* (November 2011), 1–16, doi:10.1029/2011WR010542.

Raleigh, M. S., C. C. Landry, M. Hayashi, W. L. Quinton, and J. D. Lundquist (2013), Approximating snow surface temperature from standard temperature and humidity data: New possibilities for snow model and remote sensing evaluation, *Water Resour. Res.*, *49*, 8053–8069, doi:10.1002/2013WR013958.

Ralph, F. M., P. J. Neiman, and R. Rotunno (2005), Dropsonde observations in low-level jets over the Northeastern Pacific Ocean from CALJET-1998 and PACJET-2001: Mean vertical-profile and atmospheric-river characteristics, *Mon. Weather Rev.*, *133*(4), 889–910, doi:10.1175/MWR2896.1.

Rice, R., R. C. Bales, T. H. Painter, and J. Dozier (2011), Snow water equivalent along elevation gradients in the Merced and Tuolumne River basins of the Sierra Nevada, *Water Resour. Res.*, *47*(8), doi:10.1029/2010WR009278.

Shamir, E., and K. P. Georgakakos (2006), Distributed snow accumulation and ablation modeling in the American River basin, *Adv. Water Resour.*, *29*(4), 558–570, doi:10.1016/j.advwatres.2005.06.010.

Van Wagtendonk, J. W., and J. A. Fites-Kaufman (1997), Sierra Nevada bioregion, *Fire California's Bioregions*, 264–294.

Welch, S. C., B. Kerkez, R. C. Bales, S. D. Glaser, K. Rittger, and R. R. Rice (2013), Sensor placement strategies for snow water equivalent (SWE) estimation in the American River basin, *Water Resour. Res.*, *49*(February), 891–903, doi:10.1002/wrcr.20100.

White, A. B., D. J. Gottas, E. T. Strem, F. M. Ralph, and P. J. Neiman (2002), An automated brightband height detection algorithm for use with Doppler radar spectral moments, *J. Atmos. Ocean. Technol.*, *19*(5), 687–697, doi:10.1175/1520-0426(2002)019<0687:AABHDA>2.0.CO;2.

White, A. B., D. J. Gottas, A. F. Henkel, P. J. Neiman, F. M. Ralph, and S. I. Gutman (2010), Developing a performance measure for snow-level forecasts., *J. Hydrometeorol.*, *11*(3), 739–753, doi:10.1175/2009JHM1181.1.

White, A. B. et al. (2013), A twenty-first-century california observing network for monitoring extreme weather events, *J. Atmos. Ocean. Technol.*, *30*(8), 1585–1603, doi:10.1175/JTECH-D-12-00217.1.

Ye, H., J. Cohen, and M. Rawlins (2013), Discrimination of solid from liquid precipitation over northern Eurasia using surface atmospheric conditions, *J. Hydrometeorol.*, *14*(4), 1345–1355.

Zhang, Z., S. D. Glaser, R. C. Bales, M. Conklin, R. Rice, and D. G. Marks (2017), Technical report: The design and evaluation of a basin-scale wireless sensor network for mountain hydrology, Water Resour. Res., 53, doi:10.1002/2016WR019619.

Table 1. list of WSN sites and existing co-located instruments in the American River basin

WSN site name	Abbr.	Co-located oper. site abbr. on CDEC	Elev., m	Lat, Lon	# sensor nodes with data in WY 2014[a]
Schneiders	SCN	SCN[b]	2673	38.745, -120.067	8
Echo Peak	ECP	EP5[b,c,d] , ECS[e]	2478	38.848, -120.079	7
Mt. Lincoln	MTL		2477	39.287, -120.328	8
Caples Lake	CAP	CAP[b,c,d,e]	2437	38.711, -120.042	9
Alpha	ALP	FRN[d], APH[b,c,d,e]	2269	38.804, -120.216	10
Duncan Peak	DUN		2097	39.154, -120.510	6
Van Vleck	VVL	VVL[b,d]	2069	38.944, -120.306	6
Onion Creek	ONN	ONN[e]	1891	39.274, -120.356	10
Robbs Saddle	RBB	RBB[b,d], RBV[e]	1812	38.912, -120.379	9
Bear Trap	BTP	BTP[b,c]	1518	39.095, -120.577	8

[a]Out of 10 nodes installed at each local cluster

[b]Rain gauge. Note that SCN an VVL did not have data in WY 2014

[c]Snow depth

[d]Snow pillow. CAP had no data in WY 2014

[e]Snow course

Table 2. Rain/snow transition characteristics of the ten precipitation events[a]

Event	Duration, WYD	Mean elev. of 1 ^{o}C T_d, m	Δ elevation to -1 ^{o}C T_d, m	Mean T_d lapse rate, ^{o}C km^{-1}	Mean RMSE, m
E1	27-29	1463	328	-5.4	114
E2	49-52	1721	328	-4.7	163
E3	67-69	627	217	-6.5	177
E4	102-103	1691	336	-4.7	160
E5	121-122	1720	242	-4.8	196
E6	128-132	1681	343	-5.0	135
E7	148-157	1889	298	-5.7	146
E8	176-183	1485	298	-5.9	126
E9	206-208	1509	301	-5.7	137
E10	231-232	2011	330	-5.1	137
Mean	-	1580	302	-5.0	149
St.Dev	-	376	42	0.6	25

[a]Values are averages of hourly data over the entire event

Table 3. Partitioning of rain and snow, and area-weighted means, of ten precipitation events (cm)[a]

	WSN, All 80 nodes			WSN, 11 bins			Snow pillow		Rain gauge	
Event	ΔSWE	Total	Mean daily ΔSWE	ΔSWE	Total	Mean daily ΔSWE	ΔSWE	Total	Gauge only	Blended with WSN
E1	4.0	4.2	2.0	3.8	4.1	1.9	2.2	2.7	2.2	4.2
E2	1.9	2.1	0.6	1.9	2.1	0.6	1.5	1.6	3.5	3.6
E3	3.5	3.5	1.8	3.3	3.3	1.6	4.0	4.0	3.2	3.5
E4	0.4	0.4	0.4	0.6	0.6	0.6	0.9	0.9	0.8	0.8
E5	1.4	1.5	1.4	1.4	1.4	1.4	2.2	2.2	6.5	7.5
E6	9.3	12.1	2.3	9.0	11.9	2.3	11.5	15.3	24.5	25.3
E7	7.2	8.4	0.8	6.8	7.9	0.8	6.5	8.6	15.7	14.7
E8	17.9	19.1	2.6	16.1	17.0	2.3	10.0	11.0	15.4	19.1
E9	9.1	9.3	4.5	8.0	8.5	4.0	4.6	5.1	5.7	9.3
E10	0.5	0.8	0.5	0.4	0.7	0.4	0.4	0.8	1.7	2.2
Mean	5.5	6.2	1.7	5.1	5.7	1.6	4.4	5.2	7.9	9.0
St.Dev	5.5	5.7	1.2	4.9	5.2	1.0	3.8	4.9	7.9	8.6

[a]See Table S2 for statistics

Table 4. Daily average of μ, σ and coefficient of variation (CV) of elevation segments

	Lower 1/3		Middle 1/3		Upper 1/3		Basin >1500 m	
	WSN	Pillow	WSN	Pillow	WSN	Pillow	WSN	Pillow
Ave. daily SWE, cm	0.53	1.03	0.9	3.05	9.15	12.89	3.5	5.7
Ave. daily sigma, cm	0.49	0.64	0.78	2.14	8.61	10.64	3.3	4.5
Ave. daily CV	1.04	0.8	0.92	0.66	1.05	0.99	1.0	0.8

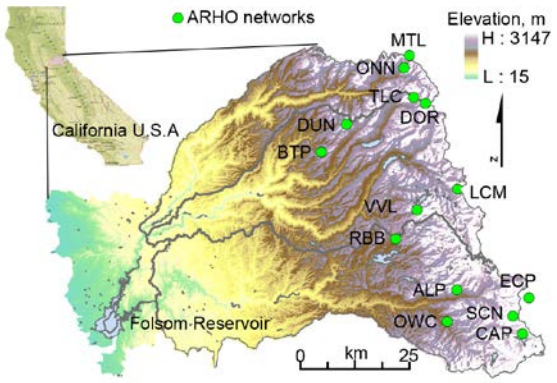

Figure 1. Location of American River basin and the 10 sensor clusters used in this analysis.

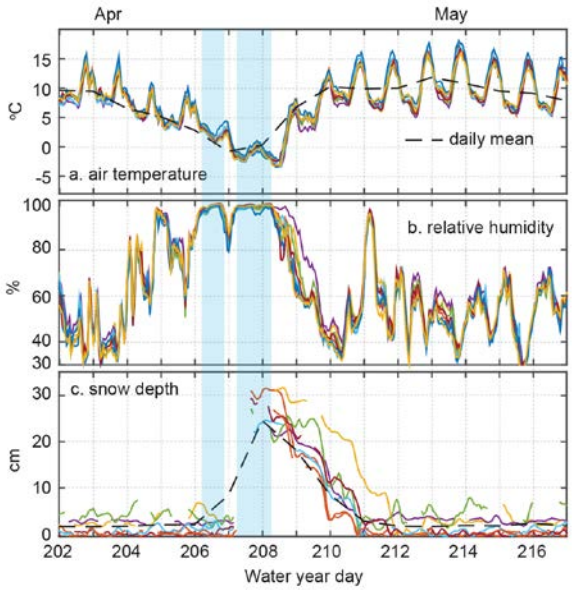

Figure 2. Measurements from the 10 nodes at ALP over 2 weeks: a) hourly and daily mean air temperature b) relative humidity, and c) snow depth. Shaded bands indicate rain (WYD 206-207) or snow (WYD 207-208) events.

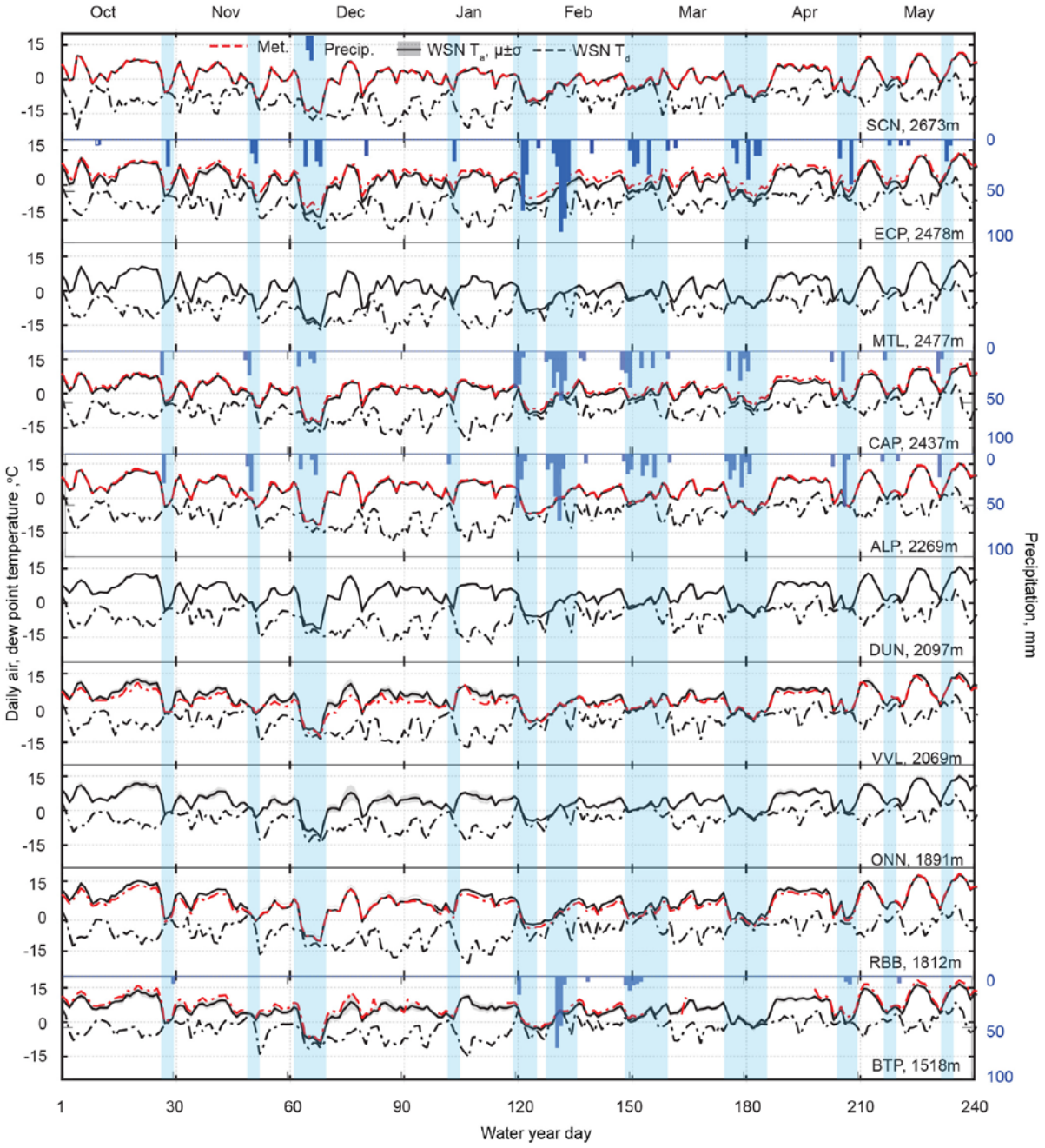

Figure 3. Daily mean air temperature (T_a), and dew-point (T_d) from sensor nodes at each WSN cluster, along with temperature and precipitation data from nearby operational met stations. Shaded areas represent periods of precipitation. See Table 2 for rain-snow transition characteristics of the ten events analyzed (E1-E10), as labeled on the bottom panel.

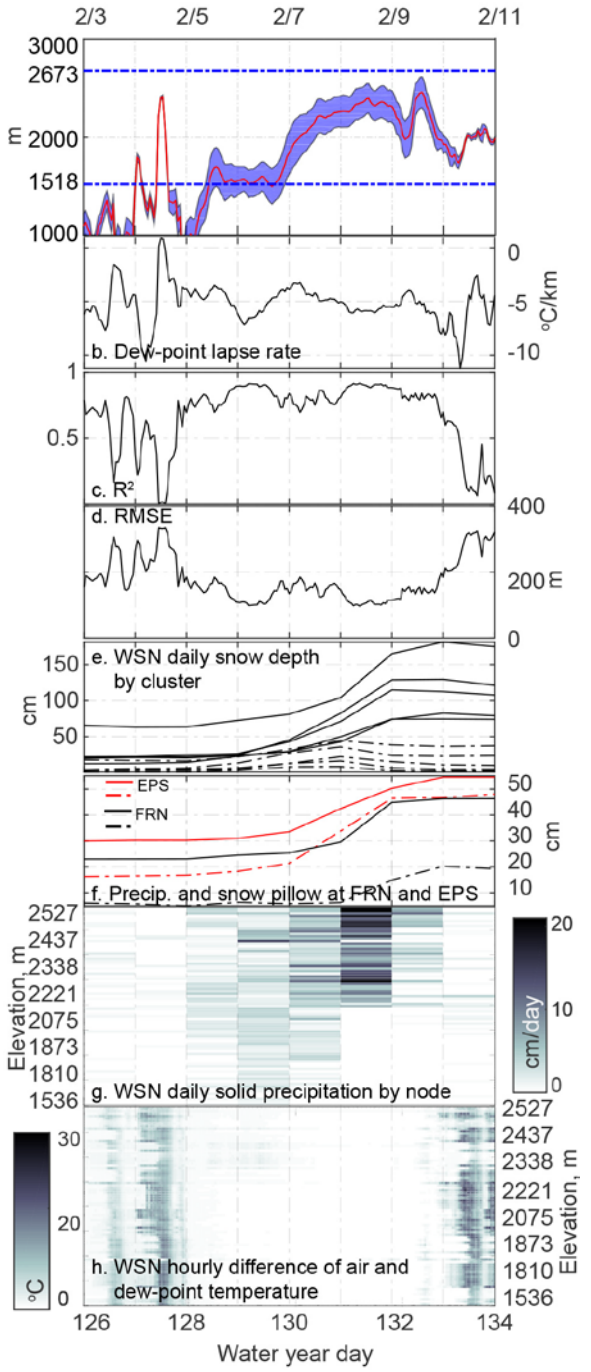

Figure 4. Characteristics of event 6: a) elevation of 0°C and ±1 °C window (shaded) of dew-point temperature, b) dew-point temperature lapse rate, based on T_d values form Figure 3, c) R^2 value of the lapse-rate fit, d) RMSE of the fit, e) daily average snow depth from the 10 WSN clusters (solid lines are for the five highest-elevation sites and dashed lines the lower five sites), f) snow-pillow and precipitation-gauge data from co-located operational sites, g) daily solid precipitation captured by WSN sensor nodes, and h) hourly differences between air and dew-point temperature.

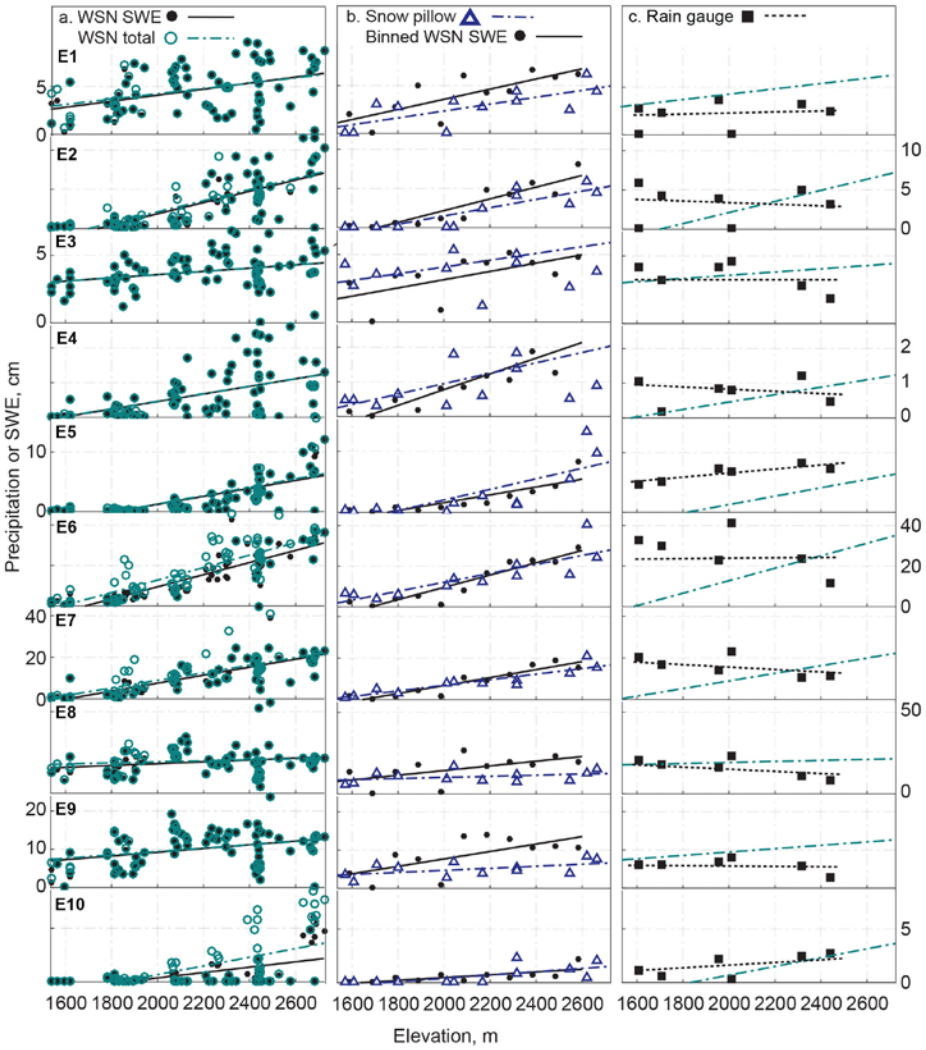

Figure 5. Comparison of SWE and total precipitation estimates as a function of elevation: a) for 80 sensor nodes within the 10 clusters, b) binned sensor nodes and snow pillows, and c) 80 sensor nodes and rain gauges. The solid and dashed lines are the best linear fit of the data. See Table S2 for statistics and slopes of lines. See Table S3 and Table S4 for a list of snow pillows and rain gauges in the American River.

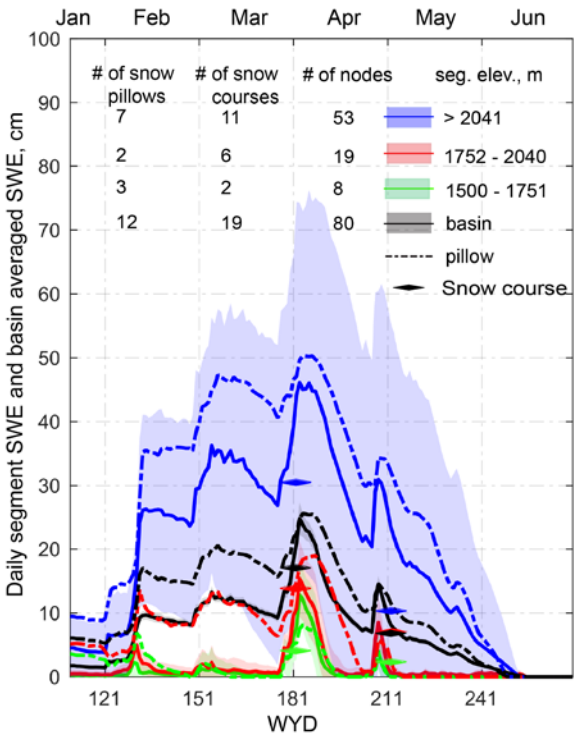

Figure 6. Basin mean SWE estimated by averaging SWE from equal-area segments above 1500 m. The shaded area represents the standard deviation of SWE estimated by WSN nodes. Also shown are basin mean SWE values calculated by snow-pillow and snow-course data, using the same method (dashed lines). See Table S5 for a list of snow courses in the American River.

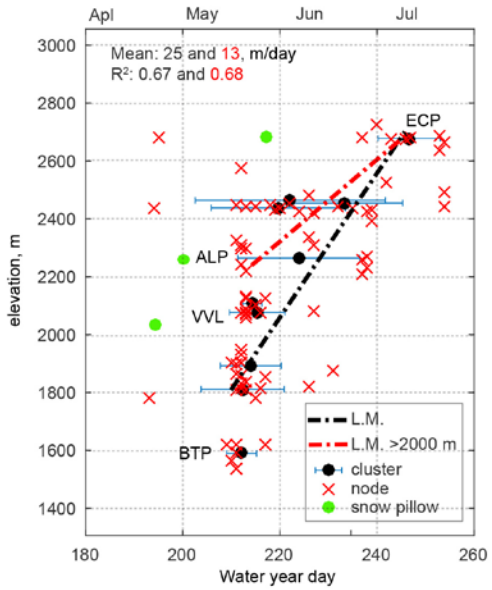

Figure 7. Snow melt-out day by elevation. The mean (scattered black circles) and standard deviation (horizontal bars) of the snowmelt progression for sensor nodes of each cluster vs. elevation. Lines are linear models for all nodes and for nodes above 2100 m elevation. Snow-pillow data also shown.

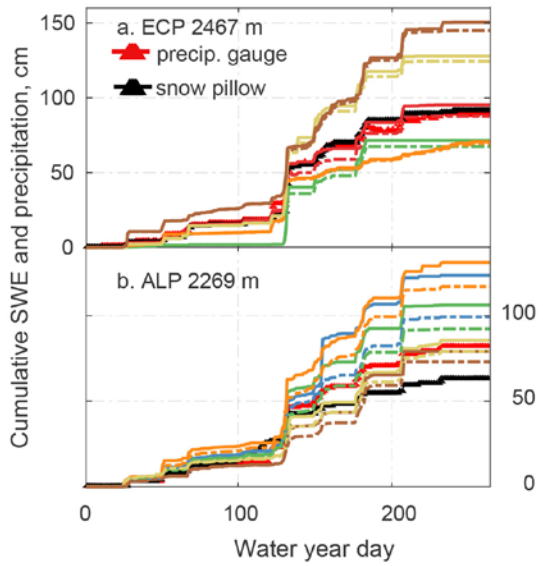

Figure 8. Cumulative solid (dashed lines) and total precipitation (solid lines) from the sensor-network nodes at ALP and ECP compared to co-located snow-pillow and precipitation-gauge data, For clarity, data from only five nodes are shown.

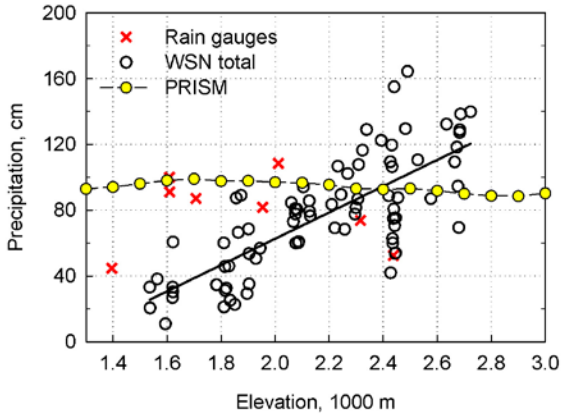

Figure 9. Seasonal total comparison of precipitation estimates, calculated as sum of all 10 events analyzed. PRISM data from http://prism.oregonstate.edu/.

Introduction

This document includes supporting tables and figures referenced in the main text.

Table S1. list of WSN sites and existing co-located instruments in the American River basin

WSN site name	Abbr.	Co-located oper. site abbr. on CDEC	Elev., m	Lat,Lon	# sensor nodes with data in WY 2014[a]
Schneiders	SCN	SCN[b]	2673	38.745, -120.067	8
Echo Peak	ECP	EP5[b,c,d] , ECS[e]	2478	38.848, -120.079	7
Mt. Lincoln	MTL		2477	39.287, -120.328	8
Caples Lake	CAP	CAP[b,c,d,e]	2437	38.711, -120.042	9
Alpha	ALP	FRN[d], APH[b,c,d,e]	2269	38.804, -120.216	10
Duncan Peak	DUN		2097	39.154, -120.510	6
Van Vleck	VVL	VVL[b,d]	2069	38.944, -120.306	6
Onion Creek	ONN	ONN[e]	1891	39.274, -120.356	10
Robbs Saddle	RBB	RBB[b,d], RBV[e]	1812	38.912, -120.379	9
Bear Trap	BTP	BTP[b,c]	1518	39.095, -120.577	8

[a]Out of 10 nodes installed at each local cluster

[b]Rain gauge. Note that SCN an VVL did not have data in WY 2014

[c]Snow depth

[d]Snow pillow. CAP had no data in WY 2014

[e]Snow course

Table S2. SNOTEL sites used in deriving snow density

Site name	Elevation, m
Fallen Leaf	1901
Truckee #2	1984
Ward Creek #3	2028
CSS Lab	2089
Echo Peak	2338
Rubicon #2	2344
Forestdale Creek	2444
Squaw Valley G.C.	2447
Independence Lake	2546
Carson Pass	2546

Table S3. Statistical results from fitting SWE and precipitation data (main text, Figure 5)

	WSN all nodes		11 bins WSN		Pillow	Gauge
Event	ΔSWE	Total	ΔSWE	Total	ΔSWE	precip.
	P-value					
E1	0.00	0.00	0.01	0.05	0.01	0.80
E2	0.00	0.00	0.00	0.00	0.00	0.72
E3	0.00	0.00	0.08	0.08	0.24	1.00
E4	0.00	0.00	0.00	0.00	0.07	0.49
E5	0.00	0.00	0.00	0.00	0.00	0.00
E6	0.00	0.00	0.00	0.00	0.00	0.95
E7	0.00	0.00	0.00	0.00	0.00	0.30
E8	0.05	0.27	0.11	0.19	0.24	0.35
E9	0.00	0.00	0.02	0.04	0.08	0.74
E10	0.00	0.00	0.01	0.01	0.01	0.16
	R^2					
E1	0.18	0.15	0.45	0.31	0.52	0.01
E2	0.56	0.54	0.72	0.71	0.76	0.02
E3	0.10	0.10	0.25	0.25	0.13	0.00
E4	0.27	0.27	0.78	0.78	0.28	0.08
E5	0.56	0.52	0.72	0.67	0.63	0.76
E6	0.77	0.70	0.79	0.77	0.70	0.00
E7	0.56	0.48	0.77	0.76	0.82	0.18
E8	0.05	0.02	0.22	0.15	0.13	0.15
E9	0.12	0.10	0.42	0.34	0.28	0.02
E10	0.32	0.35	0.49	0.53	0.49	0.30
	Slope, cm km^{-1}					
E1	3.16	2.79	4.90	3.89	3.61	0.43
E2	7.18	7.09	5.79	6.34	5.27	-0.99
E3	1.20	1.20	2.60	2.60	2.49	0.00
E4	1.09	1.08	1.61	1.59	1.50	-0.30
E5	6.71	7.06	4.33	4.40	8.90	3.29
E6	30.01	30.84	25.77	30.71	22.07	0.93
E7	19.23	18.23	18.04	20.31	13.47	-5.39
E8	5.65	3.17	12.99	10.89	3.44	-5.96
E9	4.86	4.37	10.43	8.99	2.68	-0.63
E10	2.50	4.05	1.16	2.31	1.54	1.32

Table S3. (cont.)

Event	WSN all nodes ΔSWE	WSN all nodes Total	11 bins WSN ΔSWE	11 bins WSN Total	Pillow ΔSWE	Gauge precip.
	Normalized slope, km^{-1}					
E1	0.79	0.67	1.28	0.96	1.61	0.19
E2	3.71	3.36	3.12	3.02	3.50	-0.29
E3	0.34	0.34	0.79	0.79	0.62	0.00
E4	2.53	2.47	2.66	2.58	1.66	-0.35
E5	4.64	4.64	3.19	3.06	4.00	0.50
E6	3.24	2.55	2.86	2.58	1.92	0.04
E7	2.68	2.17	2.64	2.57	2.06	-0.34
E8	0.31	0.17	0.81	0.64	0.34	-0.39
E9	0.53	0.47	1.31	1.06	0.58	-0.11
E10	5.13	4.83	3.06	3.28	3.67	0.79
	RMSE, cm km^{-1}					
E1	2.26	2.26	1.77	1.89	1.40	1.52
E2	2.15	2.19	1.18	1.31	1.21	2.53
E3	1.22	1.22	1.47	1.47	2.58	1.47
E4	0.60	0.60	0.28	0.27	0.97	0.39
E5	1.98	2.28	0.87	1.00	2.77	0.72
E6	5.59	6.81	4.28	5.49	5.89	14.21
E7	5.69	6.43	3.19	3.72	2.54	4.60
E8	8.37	8.46	8.00	8.37	3.58	5.68
E9	4.51	4.45	3.99	4.05	1.77	1.76
E10	1.23	1.86	0.38	0.71	0.64	0.80

Table S4. Snow pillow sites in the American River basin

Site name	Abbrev.	Elevation, m
Schneiders	SCN	2667
Lake Lois	LOS	2621
Carson Pass	CXS	2546
Caples Lake[a]	CAP	2438
Alpha	ALP	2316
Forni Ridge	FRN	2316
Silver Lake	SIL	2164
Van Vleck	VVL	2042
Huysink	HYS	2012
Robbs Saddle	RBB	1798
Greek Store	GKS	1707
Blue Canyon	BLC	1609
Robbs Powerhouse	RBP	1570

[a]Insufficient data for WY 2014

Table S5. Precipitation gauges in the American River basin above 1500 m

Site name	Abbrev.	Elevation, m
Schneiders[a]	SCN	2667
Caples Lake	CAP	2438
Caples (Twin) Lake[a]	CPT	2438
Forni Ridge	FRN	2316
Alpha (SMUD) [a]	ALP	2316
Silver Lake	SIL	2164
Van Vleck[a]	VVL	2042
Huysink	HYS	2012
Loon lake (SMUD)	LON	1954
Robbs Saddle[a]	RBB	1798
Greek Store	GKS	1707
Blue Canyon #2 (ETI) [a]	BL2	1609
Blue Canyon (DWR-2)	BYM	1609
Blue Canyon	BLC	1609
Robbs Powerhouse[a]	RBP	1570

[a]Insufficient data for WY 2014

Table S6. List of snow course sites in the American River basin above 1500 m

Snow course site ID	Snow course site name	Elev., m	Survey date	SWE, cm
106	Upper Carson Pass	2591	25-Mar	17.5
331	Lower Carson Pass	2560	25-Mar	17.0
107	Caples Lake	2438	25-Mar	11.5
365	Alpha	2316	2-Apr	13.5
338	Lost Corner Mountain	2286	3-Apr	11.0
108	Echo Summit	2271	28-Mar	12.0
110	Lake Audrain	2225	28-Mar	12.0
109	Silver Lake	2164	27-Mar	5.0
316	Wrights Lake	2103	31-Mar	11.5
113	Phillips	2073	1-Apr	8.0
320	Lyons Creek	2042	2-Apr	10.5
289	Tamarack Flat	1996	1-Apr	14.5
114	Wabena Meadows	1920	28-Mar	6.5
369	Miranda Cabin	1890	28-Mar	3.0
120	Onion Creek	1859	26-Mar	1.0
371	Diamond Crossing	1844	28-Mar	1.0
122	Talbot Camp	1753	28-Mar	1.5
322	Robbs Valley	1707	31-Mar	3.0
127	Ice House	1615	31-Mar	1.5

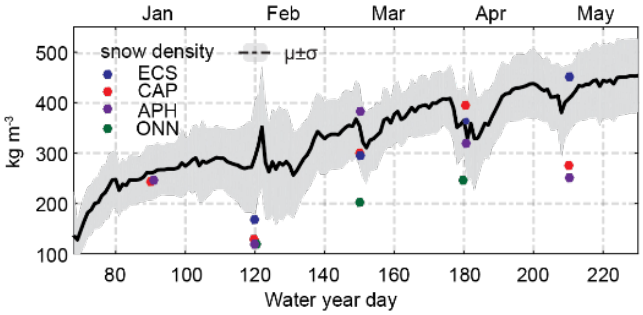

Figure S1. Basin-wide daily mean (μ) and standard deviation (σ) of snow density calculated from 9 snow-pillow sites in and around the American River basin (Table S2). We used SNOTEL sites adjacent to the American R. basin for this analysis, as the snow-pillow data in the basin had significant gaps. Densities measured by four-snow courses sites within American River basin are shown as discrete points.

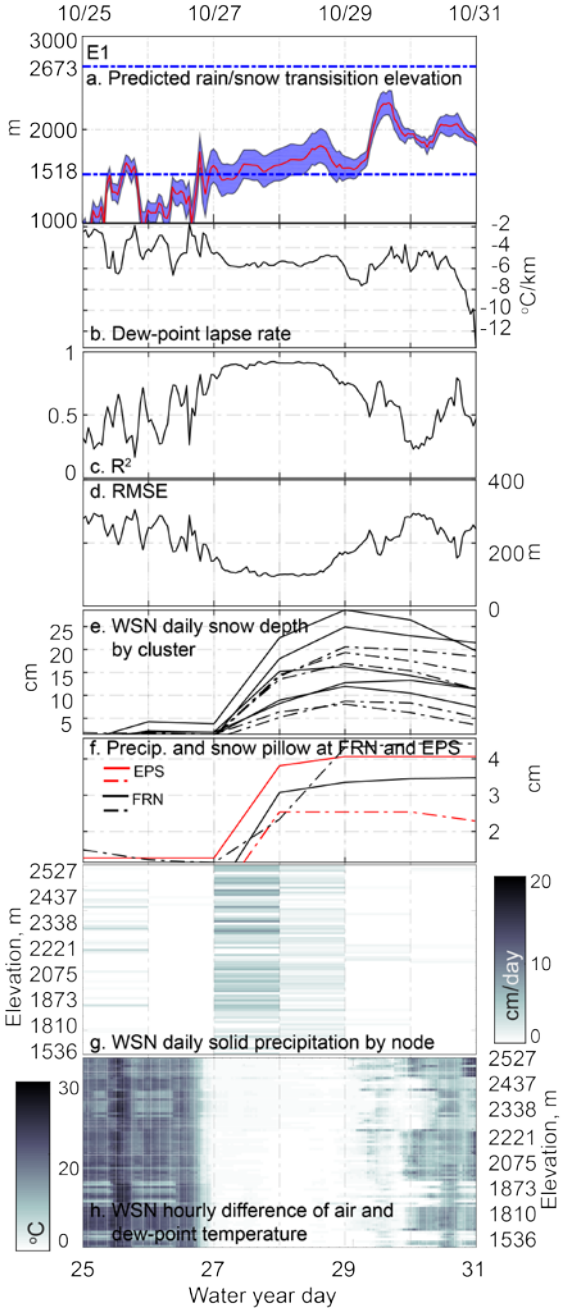

Figure S2.1

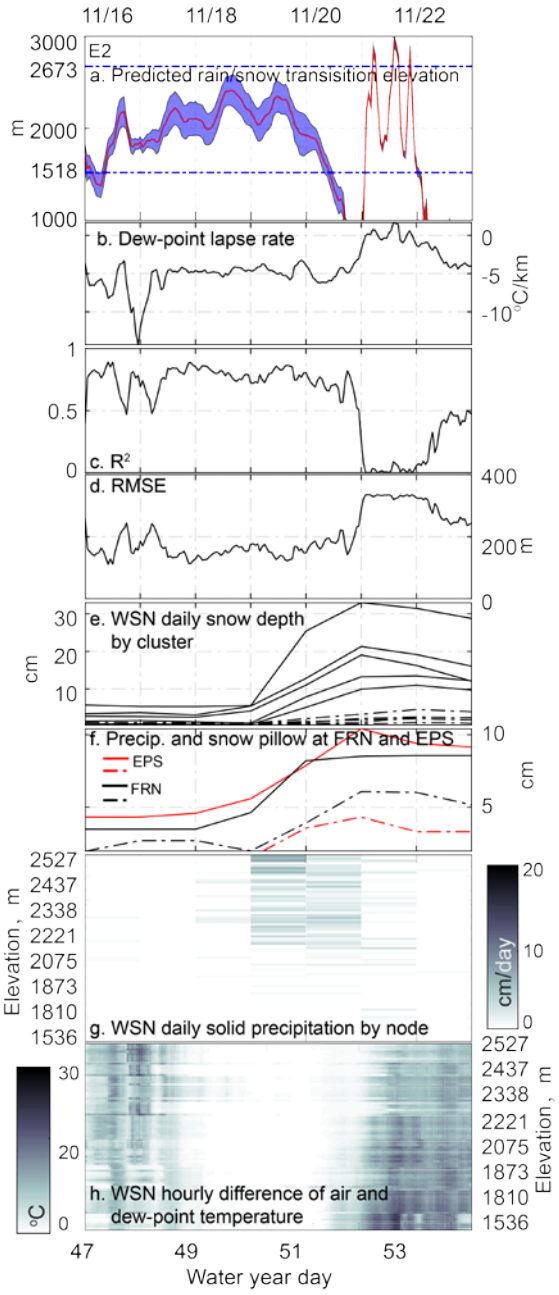

Figure S2.2

Figure S2.1-S2.9. Characteristics of event 1 to 10: a) elevation of 0°C and ±1 °C window (shaded) of dew-point temperature, b) dew-point temperature lapse rate, c) R^2 value of the lapse-rate fit, d) RMSE of the fit, e) daily average snow depth from the 10 WSN clusters (solid lines are for the 5 highest-elevation sites and dashed lines the lower five sites), f) snow-pillow and precipitation-gauge data from co-located operational sites, g) daily solid precipitation captured by WSN sensor nodes, and h) hourly differences between air and dew-point temperature.

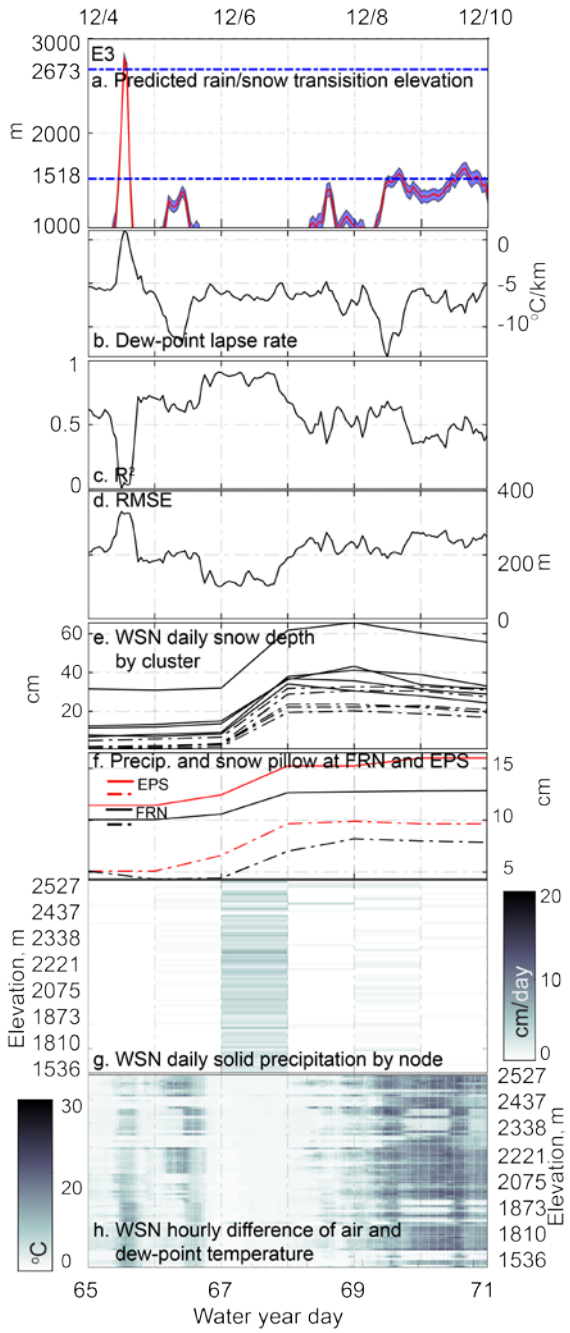

Figure S2.3

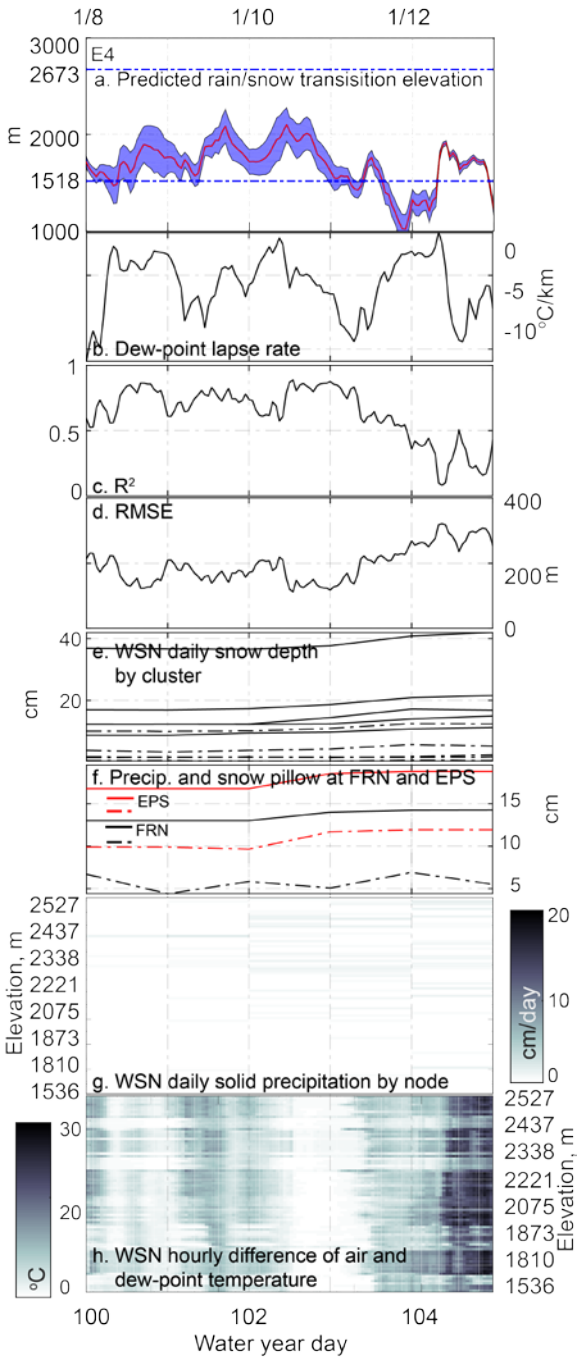

Figure S2.4

Figure S2.1-S2.9. Characteristics of event 1 to 10: a) elevation of 0°C and ±1 °C window (shaded) of dew-point temperature, b) dew-point temperature lapse rate, c) R^2 value of the lapse-rate fit, d) RMSE of the fit, e) daily average snow depth from the 10 WSN clusters (solid lines are for the 5 highest-elevation sites and dashed lines the lower five sites), f) snow-pillow and precipitation-gauge data from co-located operational sites, g) daily solid precipitation captured by WSN sensor nodes, and h) hourly differences between air and dew-point temperature.

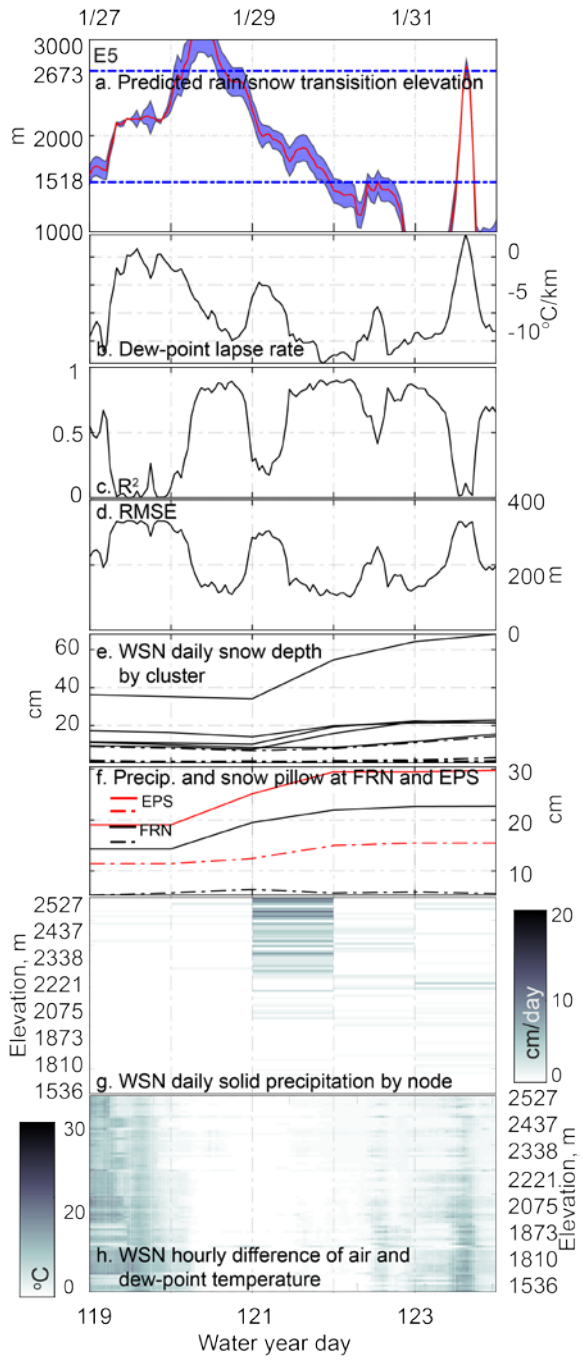

Figure S2.5

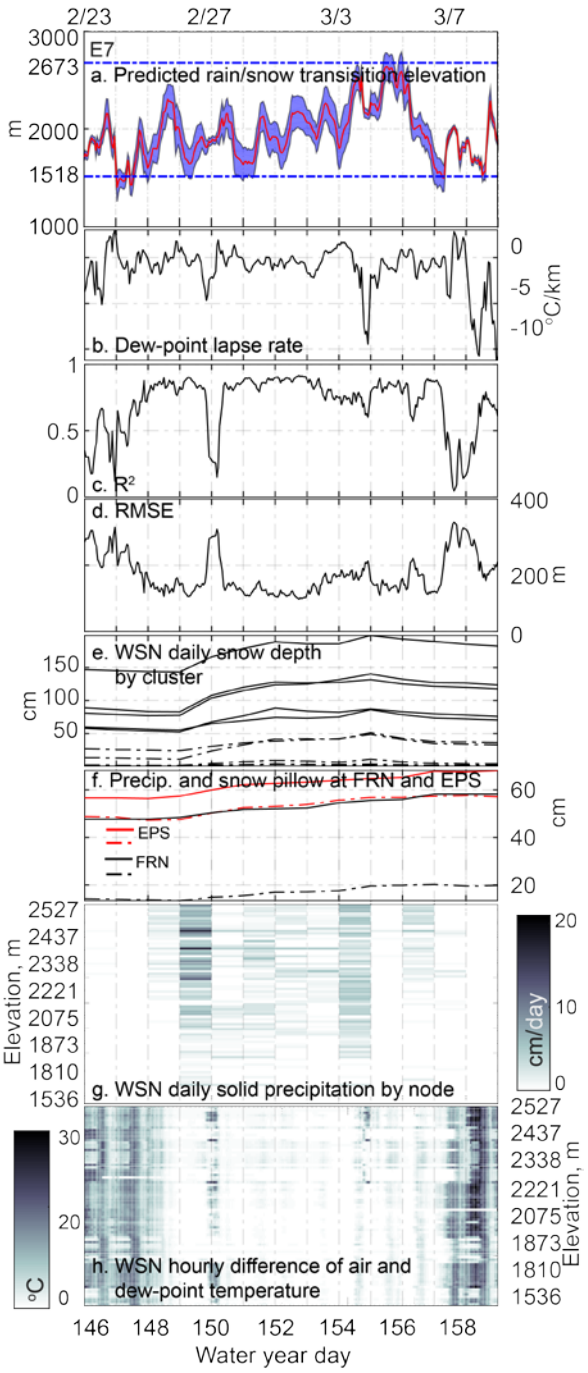

Figure S2.6

Figure S2.1-S2.9. Characteristics of event 1 to 10: a) elevation of 0°C and ±1 °C window (shaded) of dew-point temperature, b) dew-point temperature lapse rate, c) R^2 value of the lapse-rate fit, d) RMSE of the fit, e) daily average snow depth from the 10 WSN clusters (solid lines are for the 5 highest-elevation sites and dashed lines the lower five sites), f) snow-pillow and precipitation-gauge data from co-located operational sites, g) daily solid precipitation captured by WSN sensor nodes, and h) hourly differences between air and dew-point temperature.

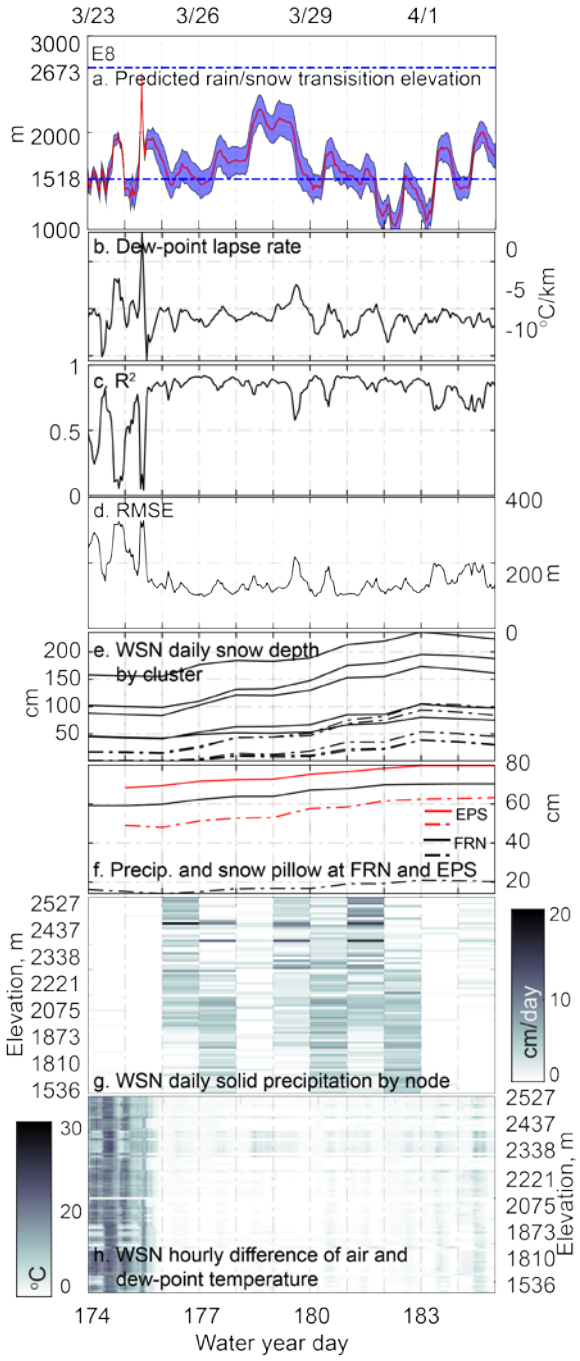

Figure S2.7

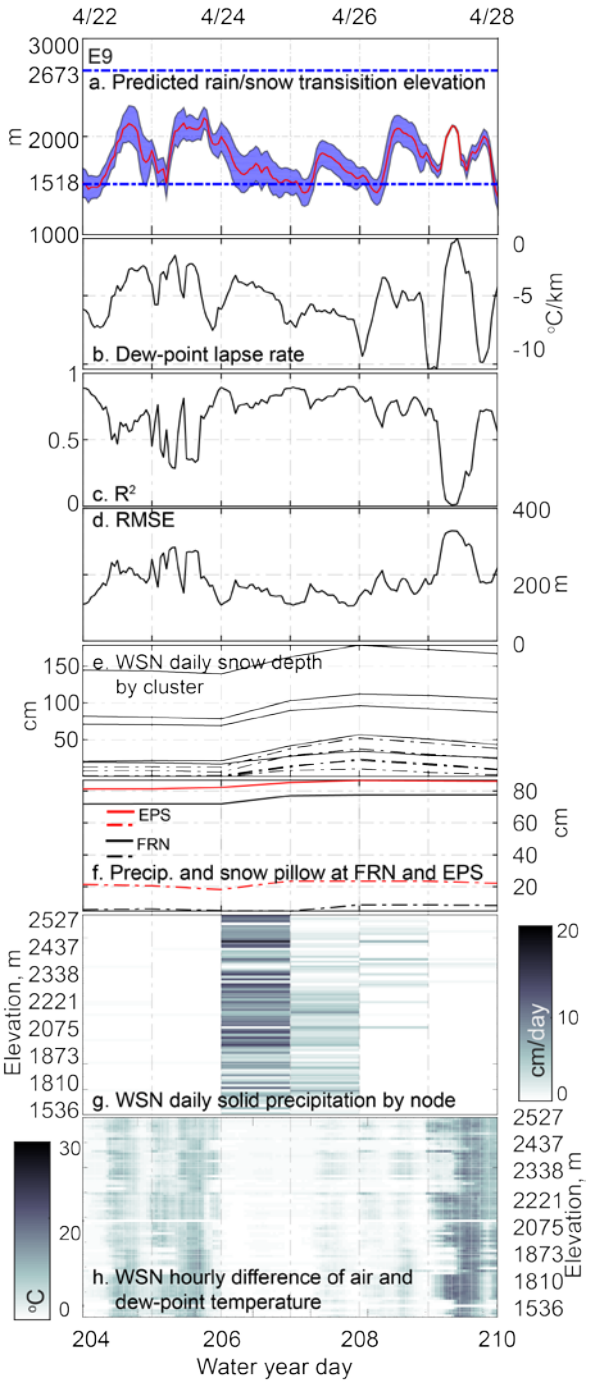

Figure S2.8

Figure S2.1-S2.9. Characteristics of event 1 to 10: a) elevation of 0°C and ±1 °C window (shaded) of dew-point temperature, b) dew-point temperature lapse rate, c) R^2 value of the lapse-rate fit, d) RMSE of the fit, e) daily average snow depth from the 10 WSN clusters (solid lines are for the 5 highest-elevation sites and dashed lines the lower five sites), f) snow-pillow and precipitation-gauge data from co-located operational sites, g) daily solid precipitation captured by WSN sensor nodes, and h) hourly differences between air and dew-point temperature.

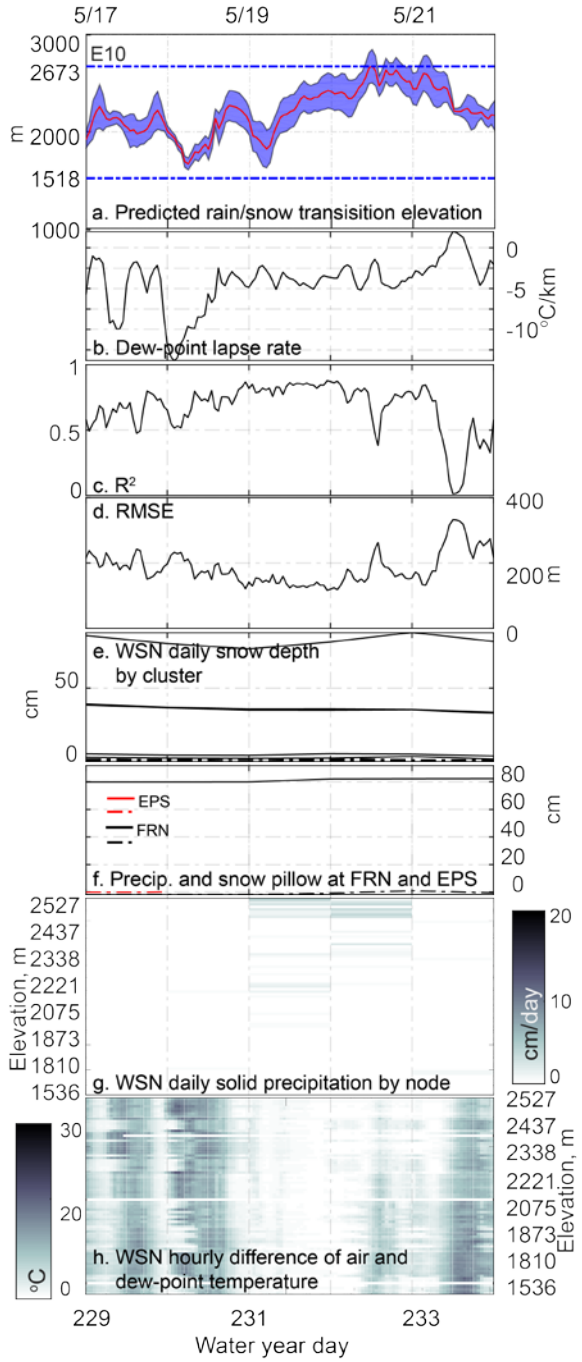

Figure S2.9

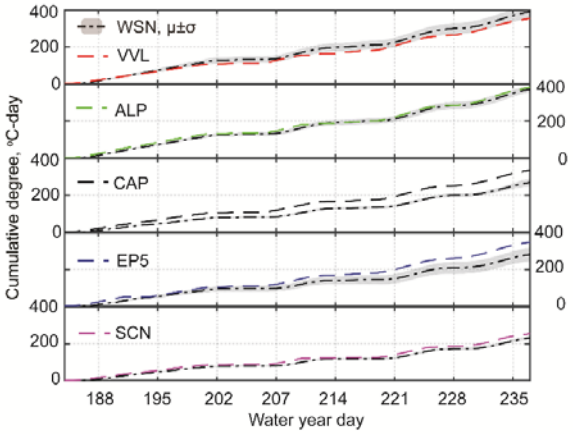

Figure S3. Cumulative degree day for WSN and the operational network at five clusters. The mean (μ) plus standard deviation (σ) are shown for the WSN sites. Data from operational-network sensors are shown in dashed lines.

Figure S2.1-S2.9. Characteristics of event 1 to 10: a) elevation of 0°C and ±1 °C window (shaded) of dew-point temperature, b) dew-point temperature lapse rate, c) R^2 value of the lapse-rate fit, d) RMSE of the fit, e) daily average snow depth from the 10 WSN clusters (solid lines are for the 5 highest-elevation sites and dashed lines the lower five sites), f) snow-pillow and precipitation-gauge data from co-located operational sites, g) daily solid precipitation captured by WSN sensor nodes, and h) hourly differences between air and dew-point temperature.